Development of a Novel Piglet Model to Simulate the Physiology of a Child with Hypoplastic Left Heart Syndrome during the First Interstage for Investigating Changes in Tricuspid Valve as it Adapts to a High-pressure and High-volume Stress Environment

by

Lily Qing Lin

A thesis submitted in partial fulfillment of the requirements for the degree of

Master of Science
in
Translational Medicine

Department of Medicine
University of Alberta

Abstract

INTRODUCTION:

Tricuspid valve (TV) failure develops in 25-35% of children with hypoplastic left heart syndrome (HLHS) and is a risk factor for morbidity and mortality. The mechanisms underlying TV failure in HLHS are not well understood. There is no effective medical therapy and current surgical strategies for TV repair in HLHS are modest in success and durability. Innovative strategies require improved understanding into the adaptive abilities of the TV.

PURPOSE:

Through the development of a novel piglet model simulating HLHS first surgical interstage right ventricular (RV) physiology, we aim to study TV adaptive changes when exposed to chronic preload and afterload stressors. We hypothesize that TV competency is maintained by adaptive rapid leaflet expansion despite annular dilation.

METHODS:

Twenty piglets (4 - 5weeks) underwent left thoracotomy. Intervention piglets (IP, n = 10) had their pulmonary valve torn to produce moderate to severe pulmonary regurgitation (volume loading) and pulmonary artery band placed to increase RV pressure. Age and gender-matched control piglets (CP, n = 10) had sham surgery. Following 4-week recovery, we performed RV pressure measurements and three-dimensional

echocardiography (3DE) of TV. TV annulus and leaflet geometry at mid and end-systole were measured using custom 3DE MATLAB software. Ex-vivo TV leaflet area was photographed and measured.

RESULTS:

All IP had severe pulmonary regurgitation, significantly elevated RV systolic pressure, thicker RV free wall and anterior papillary muscle, confirming an effective model. IP had larger and more circular annulus, but similar bending angle to CP. IP in-vivo 3DE TV leaflet surface area was 43% greater than CP, especially in the posterior leaflet. Coaptation surface area was similar while IP TV leaflet tethered volume and tricuspid regurgitation was greater. No difference in ex-vivo TV pathologic specimen (unstretched) area was detected, however correlation with 3DE TV leaflet area persisted ($r = 0.60$, $p = 0.02$).

CONCLUSION:

Exposure to chronic RV volume and pressure stressors, TV adapt by annular dilation while maintaining “saddle” shape and total coaptation surface area. This is mostly achieved through a process of rapid leaflet expansion. Further study of TV leaflet growth and its modulation may provide novel insights into the pathophysiology of TV failure in HLHS.

Preface

This thesis is an original work by Lily Lin. The research project, of which this thesis is a part, received research ethics approval from the University of Alberta Research Ethics Board, Project Name “Tricuspid valve adaptation to chronic preload and afterload (Pilot study)”, AUP Number 1999, November 14, 2016. The research conducted for this thesis forms part of a multidisciplinary collaborative project led by Drs. Nee Khoo and Darren Freed at the University of Alberta.

Acknowledgements

My deepest gratitude to everyone involved in this project. Firstly, I would like to thank my research co-supervisors and mentors, Drs. Nee Khoo and Darren Freed. Dr. Khoo for the initial research idea and challenging me to tackle this project. Dr. Freed for encouraging me to further my research training through completion of the Master's program in Translational Medicine. Through their outstanding mentorship and innovative thinking, I have learned how to be more creative with research. Both of them have set a high standard for what it means to be a clinician-scientist.

Next, I would like to thank all of our collaborators involved in this project. Dr. James Yashu Coe for his catheterization expertise and creating specially designed sheaths for this project. Dr. Timothy Colen for his 3DE knowledge and Dr. Richard Thompson for the MATLAB analysis software. Dr. Consolato Sergi for his expertise and guidance in valve histopathology. I would like to acknowledge Dr. Taisiya Sigaeva and Dr. Elena Di Martino for their skillful conduction of the biaxial mechanical stress testing on challenging valve leaflet tissue. Dr. Walter Herzog and Dr. Ziad Abu Sara for their tremendous expertise in second-harmonic generation and two-photon excitation fluorescence microscopy.

I am also grateful to Dr. Daina Domahidi for her veterinary expertise and advise through the project. Dr. Sanaz Hatami and Xiuhua (Sue) Wang for assisting me with animal care during surgery and perioperative period. I would also like to thank Deb Dixon, Ryan

Edgar and Katie-Marie Buswell, personnel at Ray Rajotte Surgical Medical Research Institute (RRSMRI), for animal monitoring as we conduct our surgical procedures.

Lastly, I would also like to acknowledge the Women & Children's Research Institute for providing funding support for this project through the Graduate studentship grant and the Innovation grant.

Table of Contents

List of Tables

List of Figures

Figure 5: Tricuspid valves with annulus opened with a cut through the posteroseptal commissure and placed on imaging stage in a relaxed state exposing the ventricular surface for photography. A) Sample tricuspid valve from a piglet who underwent sham surgery. B) Sample tricuspid valve from a piglet who underwent the intervention surgery. Features noticeable to the naked eye include the leaflets appearing more opaque and thicker chordae

Figure 6: Biaxial mechanical stress testing setup. Direction 11 is circumferential to the leaflet and 22 is in the radial direction.

Figure 7: Key findings from 3DE regarding changes in TV annular geometry secondary to increased right ventricular volume and pressure loading. The TV annulus dilated more in the lateral width direction (A) than the anteroposterior direction (B). The annular bending angle was not significantly different (C).

Figure 8: Changes in TV leaflet area as assessed on 3DE in response to increased right ventricular volume and pressure loading. There is increased total leaflet area (A) with proportionately more expansion of the posterior leaflet (B)

Figure 9: Representative membrane tension-stretch curves for CP and IP (top 2 panels). Direction 11 (red dots) is circumferential and 22 (green dots) is in the radial direction. Representative photograph of H&E sides with the fibrosa layer outlined in between the black arrows (bottom 2 panels).

List of Abbreviations

3DE = Three-dimensional echocardiography

CP = Control group

EMT = Endothelial to mesenchymal transformation

HLHS = Hypoplastic left heart syndrome

IP = Intervention group

IQR = Interquartile range

LV = Left ventricle

PBS = Phosphate-buffered saline

RV = Right ventricle

TV = Tricuspid valve

TR = Tricuspid valve regurgitation

VTI = velocity time integral

Introduction

Background

Majority of the research and innovation in cardiac valve focuses on the mitral valve, the atrioventricular valve mostly affected in the adult population by ischemic heart disease. However, in congenital heart disease and the pediatric population, disease of the tricuspid valve (TV) occurs more commonly. The impact from TV failure in congenital heart disease is significant with increased risk of morbidity and mortality in a range of congenital heart defects, such as Tetralogy of Fallot, Ebstein's anomaly, congenitally corrected transposition of the great arteries, idiopathic pulmonary hypertension, and patients with transposition of the great arteries following an atrial switch procedure [1–5]. These lesions either have congenital malformation of the TV or the cardiac physiology is such that the TV is placed under increased volume (preload) or pressure (afterload) stress. Perhaps the most vulnerable group of children to develop TV failure are children with hypoplastic left heart syndrome (HLHS). HLHS is a rare congenital heart disease where the left side of the heart is underdeveloped. As there is no cure, patients undergo a series of three major open-heart palliative surgeries to redirect blood flow such that the right ventricle (RV) pumps oxygenated blood to the body and blood flow to the lungs for oxygenation is passive. These surgeries are usually completed by 5 years of age with a 10-year survival rate of only 70% [6]. Despite a rare disease, caring for children with HLHS carries a disproportionate financial demand on the healthcare system. In a US multicenter database study, the median combined inpatient hospital cost and charges for

the three palliative surgeries alone in 2007 was estimated to be almost $700,000 per patient [7].

Impact of tricuspid failure in HLHS

In children with HLHS, it is estimated that between 25-35% will develop significant TV regurgitation (TR)[8,9]. Numerous studies that examine anatomic and physiologic determinants of clinical outcome have consistently identified the presence of moderate to severe TV regurgitation as a risk factor not only for both perioperative and interstage mortality, but also impacting long-term survival with the Fontan physiology [8,10–15]. The mechanistic etiology underlying TV failure is not well elucidated. It is presumed to be related to the TV in HLHS having to function in a chronic increased pressure (afterload) environment with prolonged periods of volume loading (preload), contrary to the low-pressure euvolumic environment of the normal TV. From a hemodynamic perspective, significant TR increases pulmonary venous pressure [16]. This is most evident in ventricular systole with elevated atrial v-wave, reducing both atrial and ventricular filling and thereby antegrade pulmonary blood flow. There is pulmonary edema with more extravascular lung water resulting in decreased pulmonary compliance and elevated pulmonary vascular resistance. There is also interplay between TV failure and RV failure whereby significant TR leads to increased RV volume loading, increases RV end-diastolic pressure and decrease systemic cardiac output. This ultimately leads to a more dilated RV and thus TV annulus, resulting in worse TR. Without

intervention, a vicious cycle of decreased cardiac output and worsening pulmonary edema occurs, along with progressive decline in RV contractility [16].

Tricuspid valve embryology

The atrioventricular junction becomes defined following rightward looping of the heart tube at around 25th day gestation [17]. Development of the atrioventricular valves occurs in concert with ventricular development and septation of the atria and ventricles [17–19]. The early heart tube has an outer layer consists of myocardial cells and an inner layer consisting of endocardial cells. These two layers are separated by an acellular extracellular matrix called the "cardiac jelly", which consist of primarily proteoglycans and glycosaminoglycans [19,20]. At around fifth embryonic week, under local signal stimulation from the endocardium and myocardium, a small group of the atrioventricular endocardial cells delaminate from the epithelial layer, invade into the cardiac jelly and change into a mesenchymal phenotype through a process called endothelial-to-mesenchymal transformation (EMT) [21,22]. Proliferation of these mesenchymal cells then form atrioventricular endocardial cushions [23]. The two principal cushions, superior and inferior atrioventricular cushions, form first. The smaller right and left lateral cushions form a few days later [24]. Both mitral and tricuspid valves are formed from atrioventricular cushions. Initially, there is a common atrioventricular junction. At the sixth embryonic week, the atria end of the common atrioventricular canal expands to meet the developing right and left atrium. The ventricular end remains communicating only with the developing left ventricle (LV). As this time, blood flows into the

developing right ventricle only through an interventricular foramen [25]. During the seventh embryonic week, there is rapid growth of the right ventricle and enlargement of the common atrioventricular canal with expansion of the atrioventricular cushions. As a result, the rightward aspect of the common atrioventricular canal becomes aligned with the right atrium and ventricle [25]. Concurrently, the primary atrial septum grows from the atrial roof towards the common atrioventricular canal with the mesenchymal cap at its leading edge. This mesenchymal cap then fuses with the atrioventricular cushions anteriorly and the dorsal mesenchymal protrusion from the dorsal mesocardium posteriorly to complete seal the ostium primum [26]. As the mesenchymal cap makes contact with the superior and inferior atrioventricular cushions, they fuse together and with septum primum, thus dividing the common atrioventricular canal into the tricuspid and mitral orifices [27]. At the same time, within the ventricles a muscular interventricular septum emerges and grows superiorly. The fused superior and inferior atrioventricular cushions expand to meet and fuses with it, then progress to drape over the muscular septum on both sides. Now, concordant atrioventricular connections are established [28]. Mesenchyme from the fused superior and inferior atrioventricular cushions give rise to the septal leaflet of the tricuspid valve and the anterior leaflet of the mitral valve [29]. The right lateral atrioventricular cushion then gives rise to the anterior and posterior tricuspid valve leaflets, whereas the left lateral atrioventricular cushion gives rise to the posterior leaflet of the mitral valve [29]. Initially, the right side of the fused superior and inferior atrioventricular cushion, which forms the septal leaflet, is adherent to the right side of the interventricular septum. As the atrioventricular canal myocardium interdigitates with the ventricular myocardium, the right lateral

atrioventricular cushion elongates into the right ventricular cavity [27]. As the right lateral atrioventricular cushions elongates, maturation occurs through remodeling to form primitive thin anterior and posterior tricuspid valve leaflets through cell proliferation at the growing edge with apoptosis at the base of the endocardial cushion [30]. Muscular connections with the ventricular myocardium remain at the leaflet free edges as papillary muscle attachments [27]. Interestingly, the TV leaflets are not formed at the same time. The septal leaflet begins to delaminate from the ventricular septum through apoptosis of the underlying myocardium after development of the anterior and posterior leaflets. There is evidence that this process continues even after embryogenesis is complete [18]. Valve leaflets continue to thin, elongate and increase in circumferential size concomitant with growth of the ventricle. The mature trilaminar valve leaflet structure does not fully develop until after birth [31]. The atrial surface of leaflets, called the atrialis layer, contains elastic and collagen fibers. The ventricular side of leaflets, called the fibrosa layer, contains densely packed type I collagen fibers, providing leaflet strength. The central layer, known as the spongiosa, is filled with proteoglycans and glycosaminoglycans. Its role is to absorb energy associated with valve closure [32].

Formation of the valve annulus occurs through ingrowth of fibro-adipose sulcus tissue at the atrioventricular groove between the atrioventricular canal myocardium and the ventricular myocardium to meet the developing valve leaflets [26]. The septal portion of the tricuspid valve annular ring is formed through fusion of the central portion of the fused superior and inferior atrioventricular cushions. It is continuous with the central fibrous body, the membranous ventricular septum and the septal insertion of the mitral

valve. [27,33]. The fibro-adipose tissue composition of the annulus allows for electrical isolation between the atrial and ventricular myocardium.

Papillary muscles derive from the ventricular myocardium. In the early developing ventricles, the walls are composed of an outer compact myocardial layer and an inner trabecular layer with multiple muscular bundles[34]. Some of these become RV trabeculations, whereas others form papillary muscles. Papillary muscles grow towards the forming leaflets. Then mesenchymal cells from the atrioventricular cushions fill gaps between papillary muscle and leaflet, forming the chordae tendineae [34].

Tricuspid valve anatomy and normal variations

In comparison with the symmetric saddle-shaped mitral valve annulus, the tricuspid valve annulus is flatter with asymmetry [35–37]. The high-point closest to the right atrium is the anteroseptal commissure and the most apical low-point is the posteroseptal commissure [38]. In comparison with the mitral annulus, it is larger and less stiff, thus it is more prone to dilatation. The leaflets are attached basally to the fibrous annulus. The basal two-third of the leaflet is rather thin, it thickens in the center and then thins towards the leaflet free edge. On the ventricular surface and at the free edge are insertion points of chordae tendineae [38].

Unlike the mitral valve where structures are more conserved, there is considerable structural variability in the TV within the general population. Majority of our knowledge

have been gained from pathological studies [39–45]. However, these studies provide only a “snapshot” of pathologies and may underestimate the range of variability within the general population. Of the three triangularly shaped leaflets in the tricuspid valve, the anterior leaflet is usually the largest and most mobile [46]. The septal leaflet has direct chordal attachment to the interventricular septum and is usually the least mobile [47]. The posterior leaflet can be variable in size and mobility [44]. Commissures provide demarcation of the leaflets and typically occur at site of papillary muscles. In addition to commissures, leaflets can also have deep scallops or clefts. Typically, the tricuspid valve has three main papillary muscles. The anterior papillary muscle is the largest, most prominent and tends to be the most consistent. It arises from the moderator band and supports the anteroposterior commissure [45,48]. The posterior papillary muscle is usually located near the acute margin between the right ventricular anterior free wall and the inferior wall. It supports the posteroseptal commissure. There is significant variability in the location, size and number of subunits or heads within the posterior papillary muscle. The medial papillary muscle (also known as the papillary muscle of the conus or muscle of Lancisi) is the smallest papillary muscle. It arises from the anterior limb of the septal marginal trabeculation, also known as the septal band. It supports the anteroseptal commissure [41,45,47]. It also marks the separation between the inlet and outlet portions of the right ventricle and the entrance of the right bundle branch into the subendocardial layer of the right ventricle [45,49]. As the right ventricle dilates, the anteroseptal commissure is the location most prone to widen with regurgitation jets. This is due to the fact that majority of the chordal attachments onto the medial papillary muscle arise from the anterior leaflet with few from the septal leaflet. There may be additional small

accessory papillary muscles with variable size and location [44]. There is further variability with papillary muscles having one or multiple heads with one or multiple chordae. Chordae tendineae are fibrous strands that attaches valve leaflets with papillary muscles or directly onto the myocardial wall [40,42,47,50]. They can vary in complexity from a single strand to a fanlike structure. Primary chordae or free edge chordae limit excursion of the valve leaflets during valve closure, particularly the free edge chordae, to prevent valve prolapse. Secondary chordae insert on the ventricular surface of the leaflet away from the free edge, usually in the rough zone or near coaptation line. Strut chordae are larger and thicker secondary chordae, they may transmit forces from the myocardium to valve annulus. Sometimes short and dysplastic secondary chordae can limit leaflet motion and prevent normal leaflet coaptation. Tertiary or basal chordae are usually short and isolated. They usually arise from small isolated papillary muscles or the myocardial wall and inserts on the base of leaflets close to the annulus.

Tricuspid valve in HLHS: morphologic variations and features associated with valve failure

Given the variability within the general population, it is not surprising that structural variability also occurs in TV in HLHS. Since the early 1980s, there have been reports of TV abnormalities in HLHS, ranging from mild TV dysplasia, cleft in septal leaflet and Ebstein's anomaly [51]. Stamm and colleagues provided the most comprehensive pathologic series describing TV morphology in 82 HLHS specimens [52]. The most common abnormalities are the leaflet abnormalities, including tricuspid valve

dysplasia of moderate to severe degree (35%), bicuspid (12.2%) or quadricuspid TV (2.4%). Accessory orifices were also noticed within some of the valves. A prominent anterior papillary muscle was consistently present in all, but the posterior papillary muscle had significant variability in size and number of subgroups. Furthermore, in 26% of the specimens, the medial papillary muscle could not be identified and the anteroseptal commissure was supported by chordae that directly attached to the crista supraventricularis. Interestingly, the authors noted differences in the support to the septal leaflet free-edge depending on the HLHS subtype and curvature of the interventricular septum. In the HLHS subtypes where the septum curves into the hypoplastic LV, septal leaflet was mainly supported by various small accessory papillary muscles arising along the septum. When the septum was either flat or curves into the RV, there were significantly higher proportion of the septal leaflet chordal support arising directly from the septum [52].

Over the last decade, our research team has been using three-dimensional echocardiography (3DE) to improve understanding of TV failure in HLHS. Gross findings in the TV associated with valve failure include increased valve annular size, change in valve geometry to a more circular and flatter shape, presence of abnormal leaflet tethering and/or prolapse, lateral displacement of the anterior papillary muscle and presence of congenital leaflet clefts [37,53–55]. In addition to structural and functional valve features, residual systemic outflow tract obstruction, right ventricular dysfunction and dyssynchronous right ventricular contraction all impacts tricuspid valve function

[56–58]. However, these cross-sectional studies do not provide information on the evolving mechanisms underlying the development of tricuspid valve failure in HLHS.

Tricuspid repair in HLHS

As annular dilation is a common feature, there are several techniques in the literature to deal with this issue, including TV bicuspidization, De Vega partial annuloplasty and the edge-to-edge technique. In 1976, Reed and Cortes [59] and Kay and colleagues [60] both published similar posterior annuloplasty technique resulting in TV bicuspidization by obliterating the posterior leaflet. In their initial series, Mosca and Bove first published their initial results with applying this technique on eight TVs in HLHS with only one requiring valve replacement at 2-year follow-up for progressive TR [16]. Over the next decade, TV bicuspidization became the preferred technique utilized by the Michigan group for annular dilatation. However, even in the most experienced hands, this technique has a failure rate between 20-30% [61–63]. The De Vega annuloplasty involves placing pledgetted annuloplasty sutures from the anteroseptal commissure along the anterior leaflets until just past the posteroseptal commissure and tying the suture over a Hegar dilator calibrated to 2-3mm larger than the expected annulus size for the child based on normograms [64]. This technique is preferred by the group in Atlanta and although this technique was also effective at reducing regurgitation in the majority of HLHS patient operated, at 10-years approximately a third of the repaired patients developed significant residual valve regurgitation [65]. The edge-to-edge technique involves suturing together the free edge of the septal and anterior leaflets to create a

double orifice tricuspid valve [66]. Ando and Takahashi described good medium term result using this technique in their series of single ventricles with 5 HLHS patients with significant TR [67]. With the structural variability that exists in TV of HLHS, most surgical centers use a combination of these techniques along with commissuroplasties, closure of clefts and reports of anterior papillary muscle repositioning performed by the group in Boston [68]. The procedures used are guided by any structural abnormality noted in the tricuspid valve and location of the regurgitation jet on echocardiogram, as well as direct intraoperative assessment. There are various surgical series published by teams from Boston [68], Toronto [9,12], Illinois [69], Japan [70], Germany [14] and locally in Edmonton [71,72], all suggest surgery is effective in reducing the severity of valve regurgitation, but repair durability is poor with approximately 30-40% requiring TV re-operation or replacement.

Mechanistic studies on valve adaptation

There has been a recent paradigm shift in our perception of heart valves based on mitral valve research. Components of the heart valves are no longer view as unrelated inert fibrous tissues moving to changes in chamber pressures. Instead, the new concept consists of a synchronous functioning valve unit consisting of the annulus, leaflets, chords and papillary muscles with each component capable of actively adapting to changes in loading stress. In an adult sheep model, investigators were able to demonstrate rapid mitral valve leaflet expansion (17% after 60 days) and associated thickening and lengthening of chords following experimentally induced leaflet tethering without causing

mitral regurgitation [73]. These features were accompanied by histological changes and altered endothelial cell surface protein expression, suggesting reactivation of the embryonic developmental process: endothelial-to-mesenchymal transformation. Histological studies have also shown the annular third of the mitral valve aortic (or anterior) leaflet is invaded by muscle elements of atrial origin [74] and provides transient increase in tensile strength of the mitral valve leaflet [75]. In addition, there appear to be other contractile elements in the distal two thirds of the leaflet (the leaflet belly and edge), separate from the atrial muscle elements in the annular region [76]. Studies have also shown dense networks of nerve fibers on the atrial layer of mitral valve leaflets with more density on the anterior leaflet [77]. These nerve fibers arise from nerve trunks located at the base of the leaflet that are continuation of atrial endocardial plexus and fans out to form a network that extends approximately two-thirds of the way towards the leaflet free-edge. Nerve terminals with varying arborization are also found on the leaflets with close proximity with blood vessels, muscle elements and endothelial cells, postulated as targets of these efferent nerve supply [77,78]. The greatest leaflet tension is achieved during isovolumic contraction [79,80] and is dependent on the presence of synchronous left atrial depolarization [81]. This ability to generate complex leaflet tension emphasizes the active role of various elements of the mitral valve unit in modulating valve competency. Embryologically, both the mitral and tricuspid valves develop from the same endocardial cushions [82]. Histological studies have shown that similar to the mitral valve, TV leaflets and chords also have important blood supply from coronary arteries and networks of nerve fiber and terminals on leaflet atrial layer and chords [77,78], which presumably play an important role in valve growth and adaptation.

Studies that suggest TV adaptation in HLHS

Our research team has evolved to look longitudinally at changes to the TV in HLHS and showed that during the first interstage, there is rapid expansion of the TV annulus and leaflets area to maintain valve competency [83], and suggest the presence of active TV adaptation. However, interestingly, those that develop significant TV regurgitation had more leaflet prolapse, suggesting dysregulation of this adaptive process may be responsible for valve failure. Our research team recognizes that investigations to further understand this adaptive process in the TV is crucial for future innovation of medical or surgical strategies in the prevention and treatment of TV failure. Direct evidence on the mechanism or pathophysiology underlying TV adaptation to valve stressors is lacking.

Current gaps in knowledge

At the current time, the literature on TV failure in HLHS are largely based on observational studies and remain descriptive, outlining features seen in those valves that are more regurgitant as compared to ones less regurgitant. Our understanding of triggers, signaling and mechanisms underlying TV adaptation is limited. We also lack sufficient understanding and ability to distinguish between what is normal remodeling versus maladaptation. A better understanding of the interplay between TV function and RV remodeling is also required.

With the modest durability of current TV repair techniques, new innovation is required. However, there is no literature analyzing those surgical techniques and their impact on the TV leaflet tension and geometry of the annulus and subvalvar apparatus. Lastly, the optimum timing of TV repair is another area of controversy as post repair RV dysfunction is associated with mortality [12,62].

To design mechanistic studies to improve our understanding of the fundamental mechanisms underlying TV adaptation, our research team realizes that the development of an animal model with similar volume and pressure stress to HLHS is required.

Limitations of the currently available single ventricle animal models

In the literature, there are three pig models of single ventricle physiology described. However, none of those models are suitable for the study of TV adaptation. Ricci and colleagues described an acute pig model of a single LV for the study of the single ventricle physiology on regional myocardial blood flow distribution [84]. In this model, the TV is completely destroyed using a balloon catheter to result in severe tricuspid regurgitation. The surgical group from Toronto described a pig model of HLHS physiology at the second palliative stage (Bidirectional cavopulmonary anastomosis, BCPA) to study if mechanical lung assist following BCPA surgery improve hemodynamics and potentially augment survival [85]. Again, this model is non-recovery and requires extensive cardiac surgery on cardiopulmonary bypass. Lastly, Holzer and colleagues described the hybrid stage I palliation surgery for HLHS in piglets [86]. This model is originally designed as a teaching tool for interventionalists and surgeons new to

the hybrid procedure. Although this is a recovery piglet model, the procedure required expensive balloon-expandable stents that would be financially prohibitive for our study. As a result, our research team has developed a novel recovery piglet model to simulate physiological conditions similar to a child with HLHS during the first interstage. Hallmark to this physiology is both increased volume (preload) and pressure (afterload) stressor faced by the RV and TV. Using this piglet model, our research team aims to assess the ability of the TV to adapt to altered stress environment. In particular, in-vivo TV annulus and leaflet geometry, ex-vivo leaflet mechanical stress properties and collagen architecture are investigated.

Study purpose and potential research implications

The first goal of this research project is to develop a recovery piglet model that will simulate the physiologic conditions (increased pressure and volume stress) of a child with HLHS in the first interstage. This model will then enable the study of TV adaptive changes to this new environment. Utilizing this model, our study aims to document changes in TV annulus, leaflet and subvalve apparatus geometry in response to increased afterload and volume load in vivo using 3D Echocardiography. The feasibility of assessing biaxial planar tensile properties on these TV leaflets and changes in TV leaflet histologic architecture on hematoxylin and eosin stain are explored.

This project is the first of its kind. By using an early infancy model, this project will contribute to the understanding of the complex adaptive changes that occur during

maturation growth. Knowledge gained from this project will enrich our understanding of the fundamental TV structure and function in young hearts. The project findings will also be translatable to other congenital heart lesions where the TV encounters either volume or pressure stressors, such as Tetralogy of Fallot with residual combined pulmonary outflow tract obstruction and regurgitation, congenitally corrected transposition of the great arteries and dextro-transposition of the great arteries following atrial switch operation. Hence, the research impact will extend beyond children with HLHS and into children and adults with other congenital heart diseases impacted by TV failure.

Hypothesis

We hypothesize that in comparison with the piglets that undergo sham surgery (control group), piglets in our model (intervention group) will have increased leaflet expansion to compensate for annular dilation as a result of increased preload and afterload stress environment. We suspect there will be differences in leaflet mechanical stress properties and altered leaflet collagen architecture between the groups.

Methods

Piglet model design

We describe a novel piglet heart model that creates a volume and pressure load right ventricle to study the tricuspid valve (Figure 1). Volume loading is achieved through disruption of the pulmonary valve to produce regurgitation. Pressure loading is created through application of a pulmonary artery band.

Inclusion and exclusion criteria

Piglets at around 4-weeks of age will be used for this model. A 4-week-old piglet has the optimal survival characteristics for the surgical procedure, recovery and interim growth, as this is the earliest age that the piglets are consistently weaned from the sow and feeding on their own. The 4-week-old piglet maturity is equivalent to human infants at 4 to 6 months, thus providing a rapid growth and maturation model. We excluded piglets with a patent ductus arteriosus (assessed by echocardiography), cardiac or extracardiac malformation, or where infectious disease is suspected. We only used two healthy piglets per sow to avoid the pitfalls of litter effect and a technician at the swine facility unaware of the study design or objectives will choose the piglets. Equal numbers of males and females will be used in the experiments.

Anesthesia and access

Piglets are fasted for solids approximately two to three hours prior to surgery. Procedural premedication of atropine (0.04mg/kg), midazolam (0.2mg/kg) and ketamine (2mg/kg) is given through an intramuscular injection. They also receive a slow-release

preparation of buprenorphine (0.01mg/kg) subcutaneously for perioperative analgesia. Standard endotracheal intubation is performed. Piglet receives inhaled isofluorane (2-5%) for anesthetic during the surgical procedure. Initial ventilator was set to a PEEP of 4cmH2O, tidal volume between 8-10ml/kg and inspiratory to expiratory ratio of 1:1. The ventilator rate ranges between 26-36/min, adjusted to achieve pCO2 between 35-42mmHg on an arterial blood gas prior to hemodynamic measurements. Piglet is positioned initially on its back with hair shaved, surgical field cleaned and skin prepared using Betadine. Central catheters are placed in both the carotid artery and internal jugular vein for pressure monitoring, blood sampling and venous access during the procedure for medication delivery. Ventilator settings adjustments are made in response to arterial blood gas taken from the central arterial line and analyzed using a point-of-care iSTAT blood gas analyzer (Abbott Laboratories, IL). Prior to thoracotomy, we provide a single intravenous dose of cefazolin (30mg/kg) for perioperative sepsis prophylaxis. In addition, an intravenous dose of ranitidine (1mg/kg) is also provided for stress ulcer prophylaxis.

Bioptome disruption of pulmonary valve cusps

Piglet position is then readjusted to right lateral decubitus, exposing the left lateral thorax. A left thoracotomy is performed at the third intercostal space to ensure adequate exposure for visualization of the main pulmonary artery. Purse-string sutures are place and attached to a snare. Using a needle introducer, the main pulmonary artery is punctured in the middle of the purse-string sutures through which a wire is advanced. Over this wire, a custom-designed 7 French catheter sheath (Cordis, CA) with an

anchoring flange is advanced into position such that the purse-string sutures can be wrapped around the flange and snare can be tightened down on the flange to anchor the catheter onto the surface of the main pulmonary artery (Figure 2). Under direct epicardial 2D echocardiographic guidance (S12 probe, Philips iE33), a bioptome is advanced retrograde through the catheter sheath to the pulmonary valve. With direct echocardiographic visualization, the bioptome is used to secure bites into the pulmonary valve cusps causing cusp tearing and disruption of the pulmonary valve. This process is repeated until moderate to severe pulmonary regurgitation has been achieved. Pulmonary regurgitation is assessed by echocardiographic grading based on the size of regurgitation jet and Doppler profile in the right ventricular outflow tract, main and branch pulmonary arteries. We aim to achieve a regurgitant to forward flow velocity time integral (VTI) ratio of at least 0.6 in the branch pulmonary arteries at time of procedure. Once satisfied, the bioptome is withdrawn and a single lumen 5 French umbilical catheter is placed through the sheath and advanced to the RV for RV pressure monitoring during the placement of a pulmonary artery band.

Placement of pulmonary artery band

Using a silastic band, silk sutures are woven through the middle of the band for reinforcement and strength. The silastic band is wrapped around the main pulmonary artery in between the pulmonary valve and proximal to the catheter puncture site. Through direct echocardiographic guidance and direct RV pressure measurement, the pulmonary artery band is tightened and adjusted using a vascular clip to achieve ≥60% systemic RV systolic pressure. Once the desired pressure is achieved, sutures are placed

to secure the pulmonary artery band. Using the umbilical catheter, final direct measurement of RV pressure is taken. The umbilical catheter is withdrawn back into the main pulmonary artery and the pulmonary artery band gradient is calculated. Then the umbilical catheter and sheath are removed. The purse-string suture is tied off to close the puncture site on the main pulmonary artery (Figure 3). The left thoracotomy incision is closed in three layers using nonabsorbable sutures for the first layer and then absorbable sutures to close the muscle layers. Lastly, skin staples are used to close the skin layer. Bupivacaine (0.5%, max dose 2mg/kg) will be infiltrated around the skin incision. A single intravenous dose of meloxicam (0.2mg/kg) will be given prior to removal of central venous catheter for postoperative analgesia in addition to the previously given subcutaneous slow release buprenorphine. Both the arterial and venous central lines will be removed with the vessel tied off to ensure hemostasis. Hibitane cream (1% chlorhexidine) is applied to the incisions and a bandage is applied to cover the incision.

Postoperative recovery care

During the first post-operative 24-48 hours, symptoms of low cardiac output is common. The piglet spends a lot of time resting and often has difficulty maintaining body temperature without an external source of heat, such as overhead lamp or Bair hugger. It is common for the piglet not to have appetite, but it is important to maintain adequate hydration and prevent hypoglycemia through frequent offering of Gatorade and/or Ensure formula by either bottle feed or syringe feeding every 1-2 hours. For prophylaxis of incisional infection, the piglet is placed on an empiric 5-day course of oral cephalexin 30mg/kg BID. If the piglet develops significant diarrhea to the antibiotic, dose is titrated

down. The bandage dressing is left in situ for the first 24 hours, then removed, leaving the incision exposed to air. During the first week, three-times daily the incision is examined, cleaned and Hibitane cream applied. If any redness develops, it usually responds well to topical antibiotic ointment. Occasionally we have experienced superficial wound infection in the piglets which usually respond well to another course of oral cephalexin.

Postoperative pain control is well managed with twice daily oral meloxicam (0.2mg/kg) on top of the slow-release buprenorphine injection that lasts 72hours following the surgery. Oral acetaminophen (15mg/kg) is available to give to the piglets for fever and/or pain as needed. We found that while the piglet isn't feeding well immediately postoperatively, oral meloxicam can be hard on the stomach. Addition of twice daily oral ranitidine helps prevent vomiting due to gastric irritation.

Experiment design with 3D Echocardiography, histology and mechanical stress testing

Duroc breed piglets were obtained from local animal facility to undergo surgery at approximately 4-5 weeks of age, which is the human maturity equivalent of 5-6 months of age. Our research protocol was approved by the University of Alberta Institutional Animal Care and Use Committee. Twenty piglets underwent left thoracotomy. As per approved protocol, piglets in the intervention group (IP, n=10) had their pulmonary valve torn with the bioptome to produce moderate to severe pulmonary regurgitation (volume

loading) and pulmonary artery band placed to increase RV pressure as per piglet model. Age and gender-matched control piglets (CP, n=10) had sham surgery. Following a 4-week recovery period, we performed intracardiac RV pressure measurements and 3DE of TV in all piglets.

TV annulus, leaflet and papillary muscle geometry were assessed using custom designed MATLAB 3DE software (Figure 4). Using the 3DE datasets, the analysis involves division of the TV into 9 planes through the center (Figure 4B1), then on each plane, the annulus and leaflet surface is outlined (Figure 4B2). Then, coaptation points between each leaflet is outlined, dividing the entire leaflet surface plane into regions of anterior, posterior and septal leaflet (Figure 4B3). The annulus, leaflet and geometry of the anterior papillary muscle were measured at mid-systole. Then additional leaflet area measurement was performed at end-systole for calculation of coaptation index (leaflet area at end systole – leaflet area at mid-systole), an estimated measurement reflecting leaflet area involved in coaptation. Using the QLAB cardiac analysis system (Philips Healthcare) multiplanar reconstruction mode, a consistent four-chamber view was reconstructed from the 3DE datasets. In this plane, TV leaflet tenting height was measured from annulus level to the tip of the leaflets in mid-systole.

Following animal euthanasia, the entire heart was harvested and transferred to a pathology laboratory in isotonic phosphate-buffered saline (PBS) solution. In the pathology laboratory, TV tissue was harvested and placed on a stage in a relaxed state for digital photography (Figure 5). TV leaflet area was measured using Image J, Fiji

software. Then a rectangular section is cut from the middle of each TV leaflet tissue. This tissue specimen was flash frozen with liquid nitrogen and stored in -20 freezer prior to transfer frozen on dry ice to our partner collaborators in Calgary for mechanical stress testing. This freezing storage methodology has been affirmed not to significant impact on valve leaflet mechanical stress properties [87]. From the remaining TV leaflet tissue, a small rectangular strip of TV sample is cut in the radial direction to encompass annulus to leaflet tip. Each strip of leaflet sample is then formalin-fixed and paraffin embedded by a technician at HistoCore (University of Alberta, Edmonton). This technician also performed microtome sectioning and hematoxylin & eosin (H&E) staining of slides. Leaflet thickness and its ratio with spongiosa and fibrosa were measured on the H&E slides.

Frozen anterior leaflets specimens from 6 piglets (IP =3, CP =3) were thawed using PBS solution. A square sample (approximately 8mm x 8mm) was dissected from the frozen specimen. Due to limitations of working with small specimen, although the sample is taken from the middle of the leaflet, it was not possible to consistently control the selected square regions to a specific distance from the annulus. The specimen tissue thickness was determined as an average of measurements in two different locations using digital calipers. Surgical nonabsorbable pre-punched polytetrafluoroethylene (PTFE) polymer pledgets (Syneture) were glued onto the edges of the specimen to flatten the tissue sample, reinforce its edges and outline the deformable surface. The pre-punched pledget holes enable symmetric placement of two motor hooks along each respective specimen edge (Figure 6). Then, five dots were drawn onto the center of the tissue

specimen using a fine tip permanent marker to allow for stretch calculation. Then this prepared specimen was mounted on a custom designed 4-motor planar biaxial testing system (Electro-Force Systems, TA instruments, Springfeld, MO). This biaxial system simultaneously loads the tissue to 50 N/m in two orthogonal directions. The primary axes of the testing system were aligned with the circumferential and radial directions of the tissue specimen. Deformation was optically evaluated through dot tracking on a mounted camera. To ensure the tissue remained hydrated during testing, the specimen was submerged in a heated bath of PBS solution at 37 degrees Celsius for the duration of biaxial testing.

Statistics

Statistical analysis was performed on GraphPad Prism version 8.2.1 (GraphPad Software, La Jolla California USA). For each parameter, normality of the data was assessed using the Shapiro-Wilk normality test. When data were not normally distributed, between group comparisons of in-vivo 3DE TV geometry, ex-vivo TV leaflet area and H&E parameters were made using the Mann-Whitney U test with significance at $p<0.05$. As both the in-vivo 3DE TV leaflet area and ex-vivo specimen leaflet area were normally distributed, correlation between these two parameters was assessed using the Pearson correlation coefficient. No statistical testing was performed on the mechanical parameters due to the small sample size.

Results

Model validation

At euthanasia, hemodynamic assessment revealed that piglets in the intervention group (IP) continue to have severe pulmonary regurgitation. The median regurgitant to forward flow VTI ratio was 0.72 (IQR: 0.60, 0.76). The median RV systolic pressure in the intervention group piglets was 78% (IQR: 64.8, 82.5) of systemic pressure. The intervention piglets had thicker RV free wall and anterior papillary muscles. These indices confirm success in achieving an effective pressure and volume load on the RV (Table 1). Unfortunately, there was worsening of TR grade and RV systolic dysfunction in the intervention group piglets.

In-vivo 3DE and ex-vivo TV leaflet assessments

In the intervention group, the TV annulus was dilated when assessed by in-vivo 3DE. In particular, the dilation was more in the lateral width rather than the anteroposterior plane (Figure 7A and B), suggesting a more circular annular geometry. However, the annular bending angle remained similar between the intervention and control group, suggesting that the "saddle shape" of the TV annulus was maintained (Figure 7C, Table 2 in vivo annular geometry). Intervention piglets in-vivo 3DE TV leaflet surface area was 43% greater than control piglets (Figure 8A), especially in the posterior leaflet (Figure 8B, Table 2 in vivo leaflet geometry). Coaptation index was similar between the groups. The intervention group TV leaflet tethering volume was

significantly greater. Although not statistically significant, there was also a trend towards increased leaflet tenting height in the intervention group. Using 3DE, the anterior papillary muscle analysis found a 20% increase in chordal length in the intervention group and hypertrophy of the anterior papillary muscle, while the anterior papillary muscle position was not significant different between groups (Table 2 in vivo anterior papillary muscle geometry).

On gross inspection of the leaflets, accessory clefts within the septal leaflet was noticed in one of the piglets in the control group and two in the intervention group. Leaflets from the intervention group more opaque with thicker chordae tendineae (Figure 5). Unstretched total TV leaflet area was not different between groups, however, a direct correlation exists between ex-vivo specimen and in-vivo 3DE TV leaflet area ($r = 0.60$, $p = 0.02$).

Histology and biaxial mechanical stress testing

Histological assessment of TV leaflet cross-sectional thickness was not different between groups. However, leaflets in the intervention group had increased fibrosa/thickness ratio when compared with control group. The average fibrosa/thickness ratio was 0.54 (IQR: 0.49, 0.57) in interventional piglets and 0.36 (IQR: 0.28, 0.55) in control piglets ($p = 0.04$).

Biaxial mechanical stress testing was successfully performed on six anterior leaflets. Representative tension-stretch (T-λ) curves (Figure 9) from intervention and

control groups demonstrate a non-linear and anisotropic mechanical behavior with a stiffer response along the radial direction (22, green dots) of the valve for both groups. Under the same tension, leaflet from intervention piglets appear to deform more in the circumferential direction (11, red dots) as compared with leaflets from the control group. This is evidenced by a higher maximum stretch achieved in intervention pig leaflets of 1.08 (IQR: 1.07, 1.09) as compared with 1.06 (IQR: 1.05, 1.07) in control pig leaflets.

Discussion

Model development considerations and challenges

1. Age and thoracotomy versus sternotomy for surgical exposure

Prior to formulation of current piglet model, our team worked on piglet cadavers ranging from 1-week to 6-weeks of age with the goal to determine the age range where procedural instrumentation and exposure would be adequate. Our surgical procedure required direct echocardiographic guidance, so the piglet had to be of adequate size to allow for an echocardiographic probe to be placed epicardially with still adequate room to maneuver procedural equipment. From this work, we were able to determine that a left lateral thoracotomy provided the best exposure to the main pulmonary artery for the procedure. Furthermore, a piglet around 3 to 4-weeks of age was sufficiently large for the procedure. In discussion with our research veterinarian and colleagues at the Swine Research and Technology Center (SRTC) where the piglets are bred, it was determined

that a 4-week-old piglet has the optimal survival characteristics for the surgical procedure, recovery and interim growth, as this is the earliest age that the piglets are consistently weaned from the sow and feeding on their own. Ability to self-feed is important for successful postoperative care and avoidance of supplemental parental nutrition, which would require additional instrumentation and tubing to remain attached to the piglet postoperatively, posing significant potential risk of infection.

Also, piglets at around 4-weeks of age have the maturity equivalent to human infants at 4 to 6-months, thus providing an infant model with rapid growth potential and better mimics the timing of this physiology in children with HLHS as compared to a more mature model. Furthermore, when we tried to use an older piglet around 6-weeks of age, we found that with pulmonary vascular resistance falling, the RV quickly become untrained to handle acute increase in pressure applied by the pulmonary artery band. Six-week-old piglets were more hemodynamically unstable to slight changes in pulmonary artery band tightness and we were only able to achieve approximately half systemic RV systolic pressure with any further tightening of the PA band resulting in acute RV failure and low cardiac output.

2. Preoperative preparation

Piglets are transferred from breeding center to the care facility approximately a week prior to surgery for familiarization with the environment to help reduce perioperative stress. During that time, we socialize the piglet and introduced them to an oral electrolyte solution (Gatorade) and nutrition supplement (Boost or Ensure) using oral

syringe or bottle feeding. They appear to enjoy orange flavoured Gatorade and vanilla flavoured Ensure best. This socialization period better enables the piglets to tolerate the frequent clinical assessments in the immediate postoperative period and learn the skills of taking liquids through a bottle or syringe. By familiarizing them with the taste of Ensure and Gatorade, it provides us with a thin liquid to help with hydration and a liquid nutrition supplement in the postoperative period when they are not interested in their regular creep feed. In addition, all of our postoperative analgesia and antibiotic prophylaxis are given orally. The skill of taking liquids through a bottle or syringe is essential to enhanced postoperative care.

We routinely fast our piglets from their creep feed approximately 2-3 hours prior to surgery. We have found that longer fasting periods in this age group is associated with more perioperative hypoglycemia. Since our surgical field is above the diaphragm, we have not encountered significant concerns with aspiration, postoperative emesis or ileus.

3. Anesthesia and ventilation

Initially we were ventilating the piglets with an inspiratory to expiratory (I:E) ratio of 1:2. However, despite adjusting the tidal volume and ventilator rate, we had significant challenges with CO_2 retention. A review of the neonatal ventilation literature revealed evidence for initiating ventilation with 1:1 I:E ratio and increasing only if there is significant lung pathology with hyaline membrane disease [88]. We found that an I:E ratio of 1:1 provides better CO2 clearance and improved ventilation. In the initial stages of the acute model development, we performed autopsies to examine both the heart and

lung. With the change to 1:1 I:E ratio, on gross inspection we did not find significant changes to the lung parenchyma that would suggest trauma to lung.

For our perioperative analgesia, we ordered a specially compounded sustained release buprenorphine that is effective over 72 hours. Regular buprenorphine would require an intramuscular or intravenous injection once every 3-4 hours. We found that this formulation dramatically improved our postoperative care as postoperative analgesia was well-managed with just the addition of scheduled oral doses of meloxicam (0.2-0.3mg/kg daily) with additional acetaminophen (15mg/kg BID-TID) for break-through pain.

4. Pulmonary regurgitation

To safely disrupt the pulmonary valve and achieve moderate to severe pulmonary regurgitation was challenging. Initially we tried pulling an inflated balloon across the pulmonary valve hoping to disrupt the cusps. Despite trialing a Fogarty balloon and then later a cardiac catheterization high-pressure balloon, both seem to just slide past the pulmonary valve cusps without causing significant tear or disruption. We did not try using a cutting balloon for the significant risk of bleeding. Next we tried a direct disruption technique using a metallic hook fashioned from surgical snares. Unfortunately, despite echocardiographic guidance of the hook to the pulmonary valve, the resultant pulmonary regurgitation was inconsistent and often resulted in accidental puncture of the RV outflow tract and significant bleeding. Finally, we utilized a tissue bioptome, frequently used for taking endomyocardial biopsies during cardiac catheterization. It

provided us with the precision required to take bites out of the pulmonary valve cusps thereby causing adequate disruption. Using this technique, we are more consistently able to achieve the same degree of pulmonary regurgitation.

5. Circulatory support during procedure

During the procedure, periods of hypotension with cardiac manipulation will require support through intravenous infusion of inotropes. This consists of a combination of epinephrine (0.05-0.15mcg/kg/min) and norepinephrine (0.05-0.15mcg/kg/min). Prior to pulmonary valve disruption, it is important to ensure normal blood pressure prior to procedure as the acute volume loading due to pulmonary regurgitation can be poorly tolerated.

Furthermore, we have also seen frequent non-sustained atrial and ventricular ectopy with cardiac manipulation. Sometimes the ectopy will progress into atrial or ventricular tachycardia. Therefore, it is important to have defibrillator paddles available to treat unstable arrhythmias.

5. Pulmonary artery band

The precautions above with inotropic support and management of arrhythmias are continued during the pulmonary artery band placement. We found that using vascular clips and gradual tightening of the band to be more successful. This process requires patience to allow for the RV to adapt to the acute increase in afterload. The style of securing the pulmonary artery band turned out to be very important. During the 4-week

recovery period, our piglets undergo rapid growth resulting in more than tripling of its weight. Initially, a single suture was tied around the two ends of the pulmonary artery band. This is the usual technique for pulmonary artery banding performed in children. However, after several recovered piglets were sacrificed at 4 weeks post initial procedure, we found the pulmonary artery band was disrupted (opened) prior to experimental end-point from the suture tearing through the silastic band, presumably secondary to the rapid growth of the piglet. The successful model required a thicker silastic band with hand-sutured reinforcement of the band with a circumferential suture for added strength.

In-vivo 3DE assessment of TV geometry

This project is the first to provide direct evidence for structural changes to the TV in response to increased volume and pressure loading stressors in a rapidly growing infant animal model. Our model demonstrates that as TV annulus dilates under the volume and pressure stressor, it assumes a more circular geometry. This feature is consistent with prior studies assessing the TV annular geometry in children with HLHS [37,54]. Despite annular dilatation, similar annular bending angle is maintained in the intervention group. The bending motion or "saddle-shape" of an atrioventricular valve annulus is an important element of annular function because it directly impacts stress exerted onto valve leaflets and contributes to valve dysfunction [89]. A rapid increase in total leaflet surface area is observed in our intervention group. Findings of similar coaptation index between groups suggests that the increase in atrial surface leaflet area is leaflet growth and expansion, not leaflets being more "pulled apart" with a resultant

decrease in leaflet coaptation area. Furthermore, chordal lengthening and anterior papillary muscle hypertrophy is observed in the intervention group but the relative papillary muscle position with respect to the ventricle and leaflet remains similar between groups. There is also increased leaflet tethering volume in the intervention group which results from a combination of the TV leaflet coaptation occurring slightly lower (trend towards increased tenting height), a dilated annulus and expanded atrial leaflet surface below the annulus. This finding would suggest that the degree of chordal lengthening observed may lag in compensating for the rapid annular dilation. Findings of increased TR and worse RV systolic function in the intervention group mimics the real-life scenario of progressive TR development in some HLHS children. However, specific to our hypothesis testing, these are confounders. It is interesting to find worse TR in the intervention group despite whole valve coaptation index being similar. There is also a similar lack of coaptation index relationship to TR grade in a previous HLHS study [83].We suspect that whole valve coaptation index is likely not a sensitive marker for regional malcoaptation that may be responsible for the worsening TR in the intervention group.

Concurrent to the development of the piglet model, our group was also assessing longitudinal changes to the TV through 3DE in a cohort of children with HLHS without development of significant TR or RV failure during the first interstage [83]. 3DE images were obtained before the Norwood-Sano procedure and compared with 3DE images obtained before the subsequent Glenn procedure. The findings of a similar increase in

annulus area, leaflet surface area and leaflet tethering volume provide some clinical validation of our animal model findings.

In the literature, a flatter TV annulus and lateral displacement of the anterior papillary muscle have been associated with severe TR in HLHS [37,54,83]. Perhaps a more obtuse annular bending angle and anterior papillary muscle displacement are signs of TV maladaptation. The findings of increased TV tethering volume before the Norwood procedure and increased TV prolapse volume before the Glenn procedure in association with worse TR in HLHS [83,90] further suggest that dysregulation of the leaflet expansion and chordal lengthening process may have a role in TV maladaptation. With more experiments conducted and increase in sample size, subgroup analysis of the intervention group of the piglets with worse TR and RV systolic function may provide further insights into the maladaptive process.

TV histology and mechanical properties

Structurally, the tricuspid valve is composed of three main connective tissue layers, the atrialis, spongiosa and fibrosa [32,91,92]. The atrialis layer faces the atrium and consists of collagen and elastin fibers. The spongiosa layer, rich in glycosaminoglycans and proteoglycans, is responsible for keeping the leaflet supple and reduce shear stress between the fibrosa and atrialis layer as they deform during leaflet motion [93]. The fibrosa layer is composed of a dense network of type I collagen fibers and provides strength to the leaflet. Form and function are integrally related: the leaflet

microstructure determines its anisotropic properties and affects leaflet function. Our preliminary biaxial mechanical stress testing has revealed a highly nonlinear tension-stretch behaviour of TV anterior leaflet (Figure 9 upper panels). The leaflets appear to be more compliant at the beginning of the load testing and then transition to become stiff. This nonlinear stress-strain relationship of the TV leaflet is consistent with other reports of biaxial mechanical stress testing performed on adult porcine TV [94,95]. The current accepted etiology underlying this nonlinear relationship is based on theories of collagen fiber recruitment [96,97]. In addition, it is found that the adult porcine TV is stiffer in the circumferential direction [94,95]. In contrast, we have found the infant piglet TV demonstrate a stiffer response in the radial direction when compared with circumferential. This difference is even greater in TV of intervention piglets (Figure 9 top panels). To my knowledge, there is no reported literature on the mechanical stress properties of infant porcine TV. Considering the increase in TV annulus with developmental change and somatic growth, it could be conceivable that infant piglet TV possess more flexibility in the circumferential direction. Interestingly, our preliminary histologic analysis has shown that TV exposed to chronic RV pressure and volume load have a proportionally thicker fibrosa layer. The deformation pattern of the intervention piglet TV leaflets may suggest increased proportion of collagen fibers within fibrosa along the circumferential direction. Although our preliminary data require further validation, it highlights rapid collagen formation as a potentially important area for further study into TV adaptation or maladaptation.

Limitations of the model and experimental design

The greatest shortcoming of our model is that our piglet hearts have a normal size and functioning LV which may impact generalizability to the HLHS population. Concurrent with normal LV size, the TV in our piglets also have a normal septal leaflet size. We are unable to model RV-LV interactions that occurs in HLHS variants with different LV size. Specifically, we cannot model the changes in TV function due to differences in septal leaflet size as it adapts to increased pressure and volume environment. Laohachai and colleagues have recently provided data that suggest HLHS variants with a small LV size is associated with more severe TR and worse TR progression [98]. Unfortunately, due to their study being a retrospective cohort, the investigators were unable to demonstrate an association between LV size and either RV function, TV geometry or assess the subvalvar apparatus to provide a mechanism for their findings. However, there have been other reports in the literature that may suggest similar finding with mitral atresia HLHS variant being identified as a risk factor for future TV interventions [9]. Furthermore, recall from pathologic specimens Stamm and colleagues have noticed difference in the TV septal leaflet subvalvar support apparatus in the mitral and aortic atresia HLHS variant which is associated with a small LV size and a septal position that is concave into the LV [52]. Although interesting observations, the underlying mechanism requires further exploration.

Due to working with small specimens, our inability to entirely be consistent in selecting the same square region of leaflet for mechanical stress testing is a limitation.

However, our samples are taken from the “middle of the TV leaflet”. A recent study assessing regional differences in biaxial mechanical properties in the adult pig TV has shown less variability in samples taken radially along the middle of the TV [99].

The relationship between the unstretched pathological specimen and 3DE surface area was moderate. This finding may be partly explained by the increased maximum stretched TV in the intervention piglets, increasing the difference between the in-vivo leaflet surface area and the pathologic specimen.

Future directions

Direct visualization of collagen and elastin fibers within the layers using second-harmonic generation and two-photon excitation microscopy is possible for the TV samples. Analysis of samples are currently underway. Our research team is also working on a setup to enable assessment for the TV in both relaxed and loaded states as prior research have found differences in collagen fiber orientation between the two states [100]. We hope this will provide ability for assessment of our postulated differences in collagen fiber orientation within the fibrosa layer between our intervention and control piglet groups. In adult mitral valve, it has been demonstrated that there are quiescent valvular interstitial cells that become activated under stress signaling to undergo endothelial-mesenchymal transition [32,73,101]. It is felt that this cellular process may play a role in altering collagen composition within the extracellular matrix, which may be responsible for TV adaptation. Therefore, further exploration into the leaflet cellular

function using immunohistochemistry and gene expression technologies becomes a logical next step in deciphering the mechanistic pathways responsible for valve adaptation.

Conclusion

Despite the challenges, we are successful in the development of a recovery piglet model that simulates the physiology of chronic increased preload and afterload in the right ventricle. This is especially useful for the study of children with HLHS during the first interstage as well as many other congenital heart diseases with similar physiology. Our project has found that when exposed to chronic RV volume and pressure stressors, the infant TV adapts by annular dilation while maintaining "saddle" shape and total coaptation surface area. This is mostly achieved through a process of rapid leaflet expansion. These leaflets have increased thickness of the collagen-rich fibrosa layer and appear to be stiffer in the radial direction. Further study into the mechanistic factors underlying TV leaflet growth, in particular modulation of collagen deposition within the extra-cellular matrix, may provide novel insights into the pathophysiology of TV failure in HLHS.

Figures

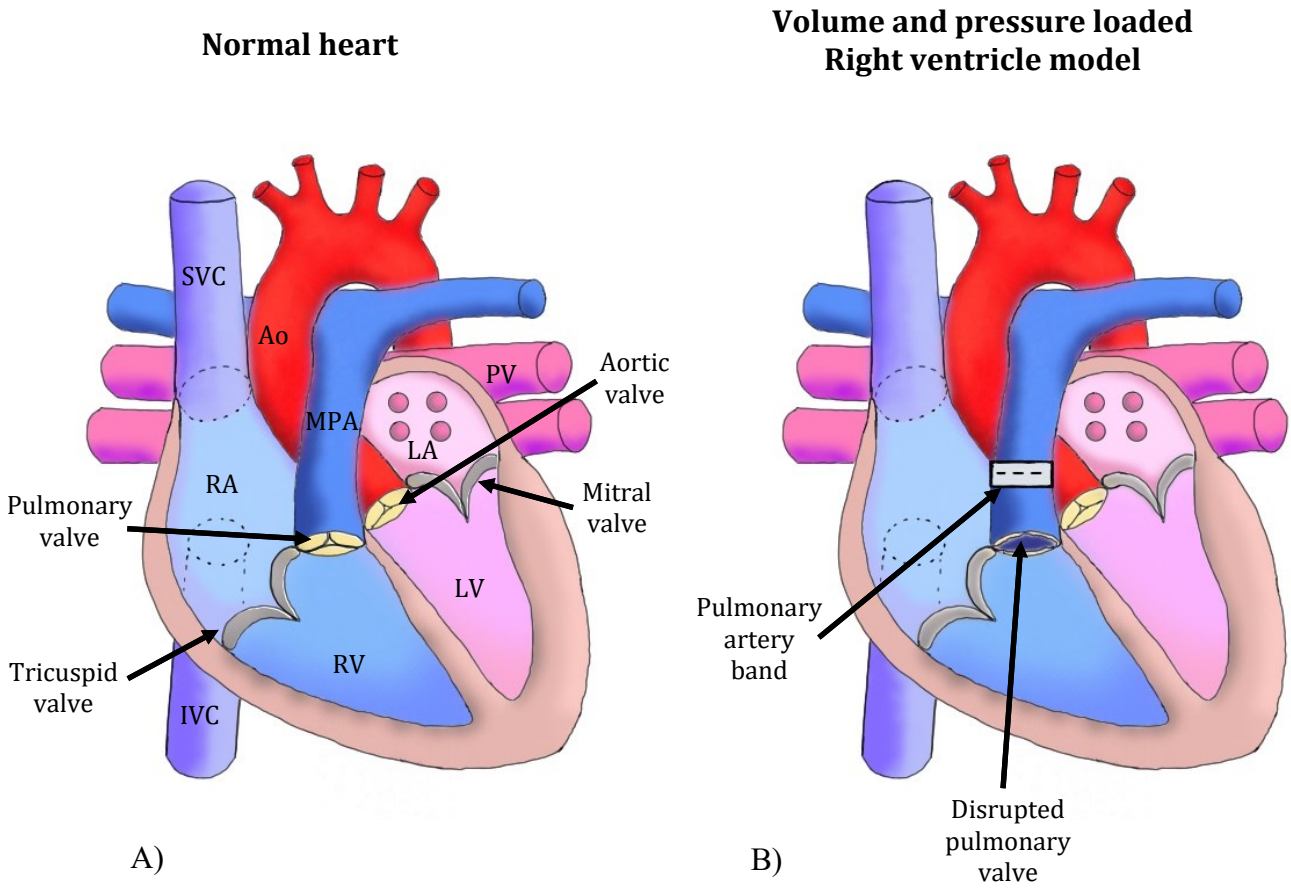

Figure 1: Diagram of a normal heart (A) and the novel volume and pressure loaded right ventricle piglet heart model (B).

SVC superior vena cava, IVC inferior vena cava, RA right atrium, RV right ventricle, MPA main pulmonary artery, PV pulmonary vein, LA left atrium, LV left ventricle, Ao aorta.

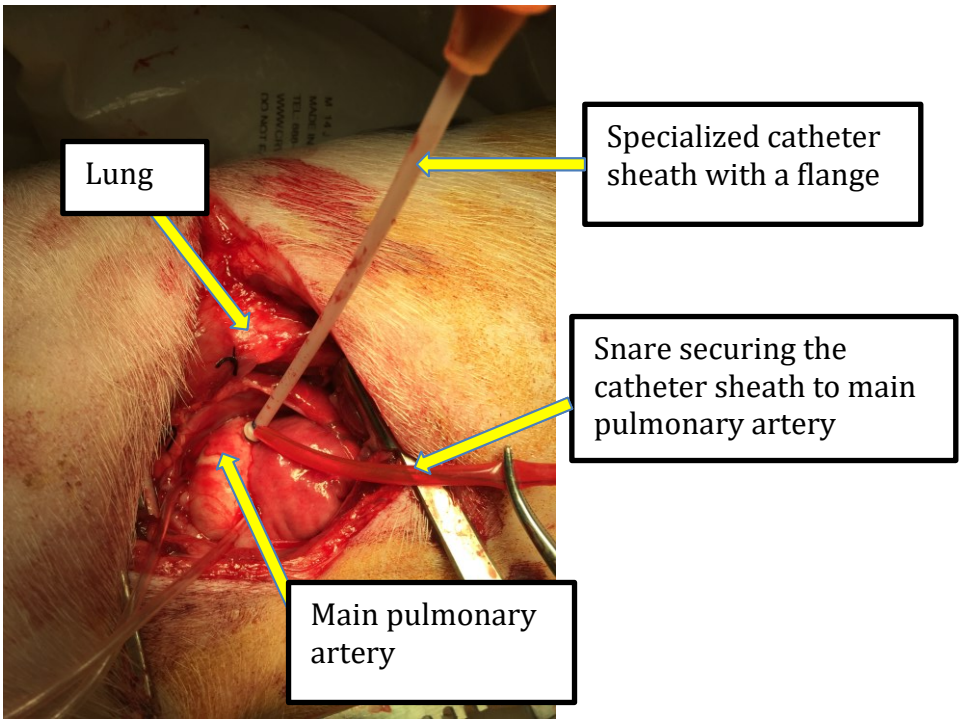

Figure 2: Intraoperative image through the lateral thoracotomy demonstrating the exposure and positioning of the specialized catheter on the main pulmonary artery to allow for bioptome disruption of the pulmonary valve.

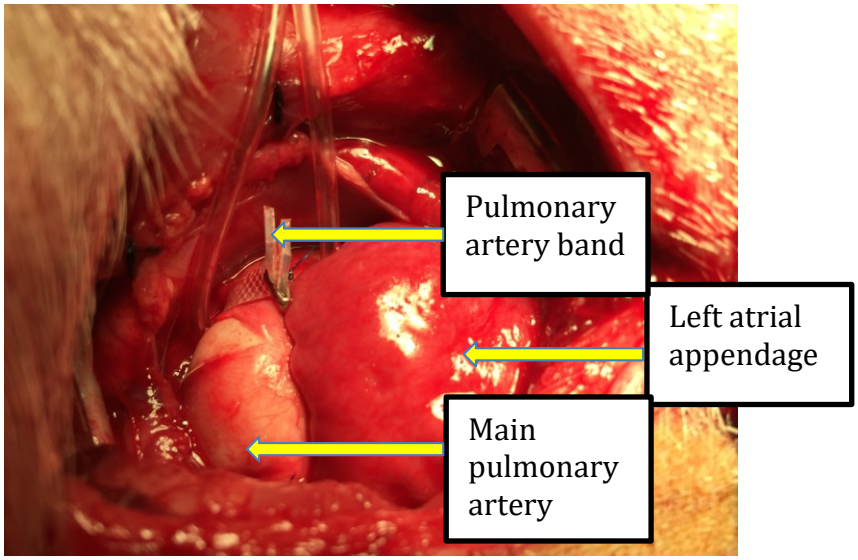

Figure 3: Intraoperative image after successful pulmonary valve disruption and pulmonary artery band placement. All of the catheters and sheaths have been removed. The main pulmonary artery puncture site has been suture closed.

A)

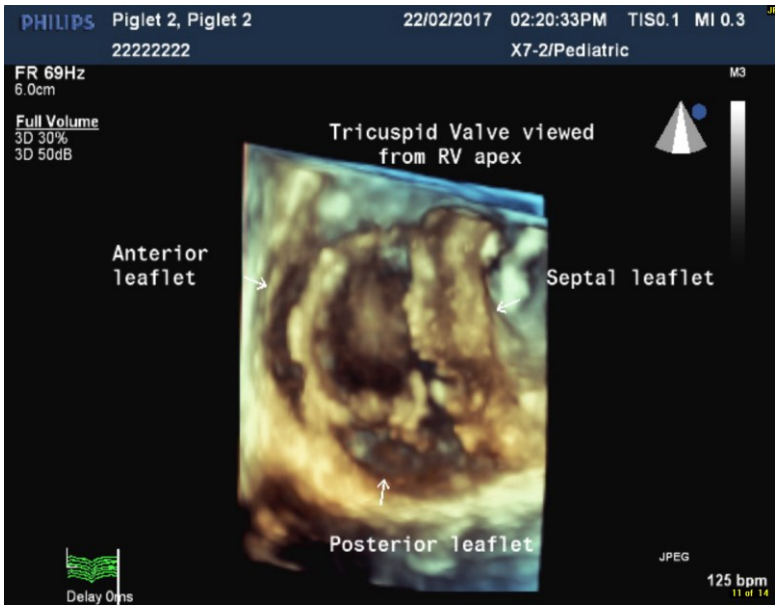

B)

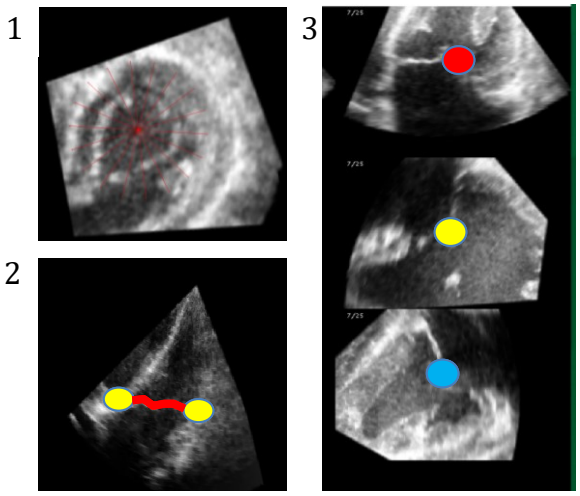

C)

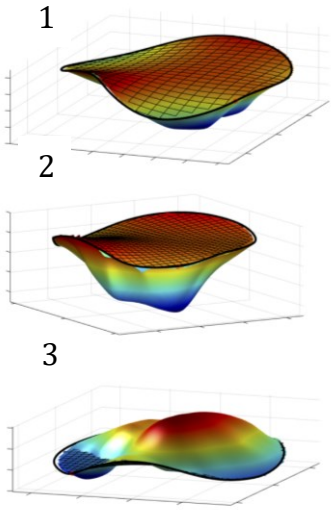

Figure 4: A) 3D-Echocardiogaphic image of the piglet tricuspid valve as viewed from right ventricular apex in the open state. B) Sample analysis of tricuspid valve 3D dataset demonstrating (1) division of valve through 9 planes, (2) tracing of the annulus and leaflet surface, (3) determining the coaptation points for division of leaflet surface map into anterior, posterior and septal leaflet regions. C) Sample tricuspid valve annular and leaflet surface geometry demonstrating (1) valve leaflet with minimal tethering or prolapse, (2) valve leaflet with large tethering volume and (3) valve leaflet with large prolapse volume.

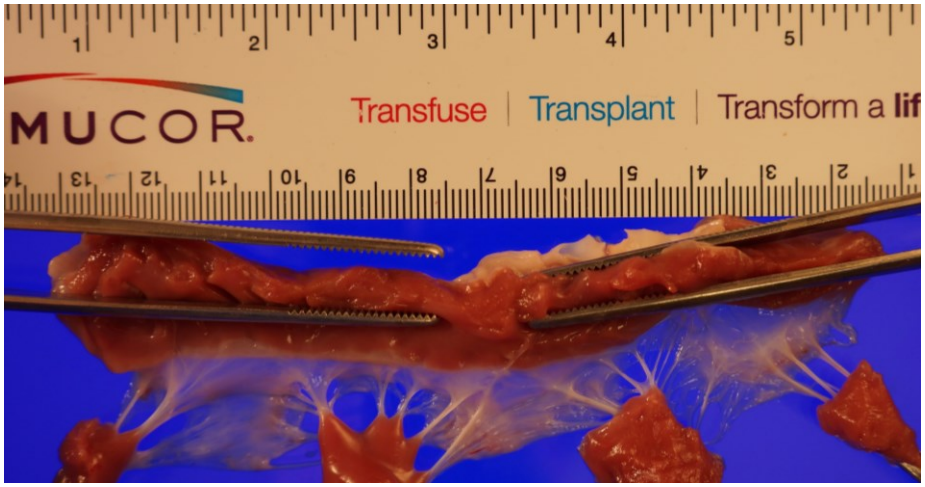

A)

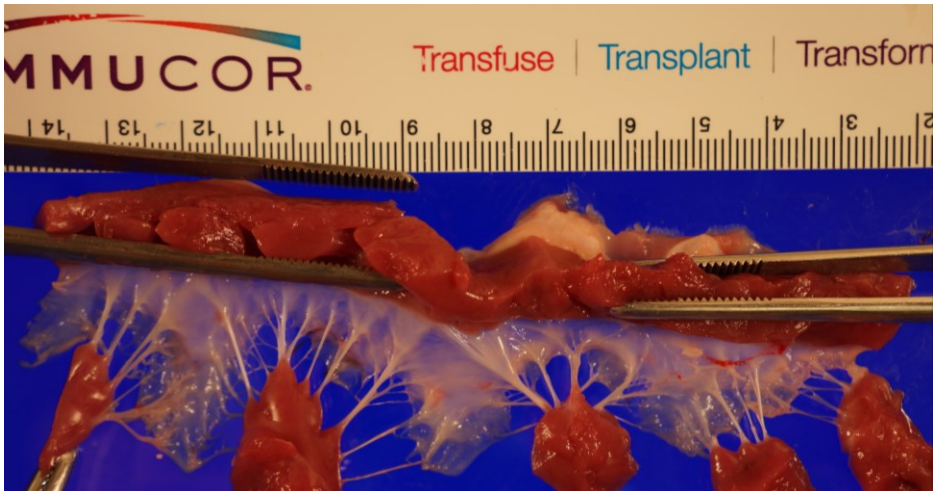

B)

Figure 5: Tricuspid valves with annulus opened with a cut through the posteroseptal commissure and placed on imaging stage in a relaxed state exposing the ventricular surface for photography. A) Sample tricuspid valve from a piglet who underwent sham surgery. B) Sample tricuspid valve from a piglet who underwent the intervention surgery. Features noticeable to the naked eye include the leaflets appearing more opaque and thicker chordae.

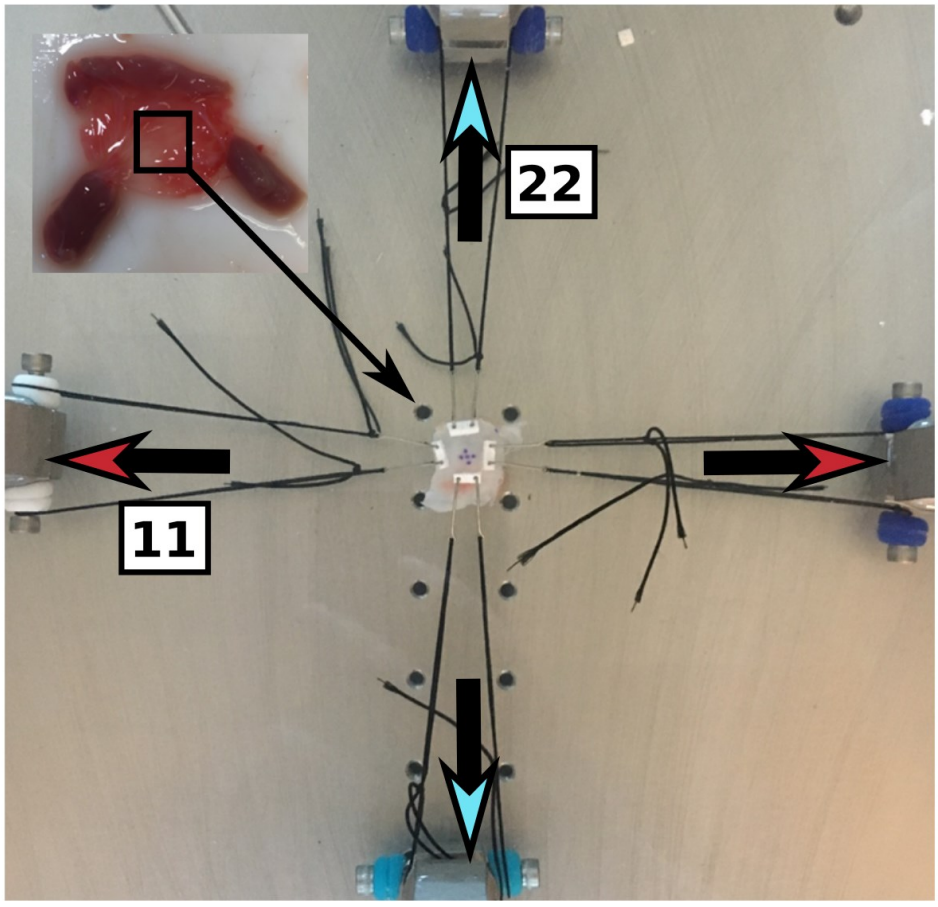

Figure 6: Biaxial mechanical stress testing setup. Direction 11 is circumferential to the leaflet and 22 is in the radial direction.

A)

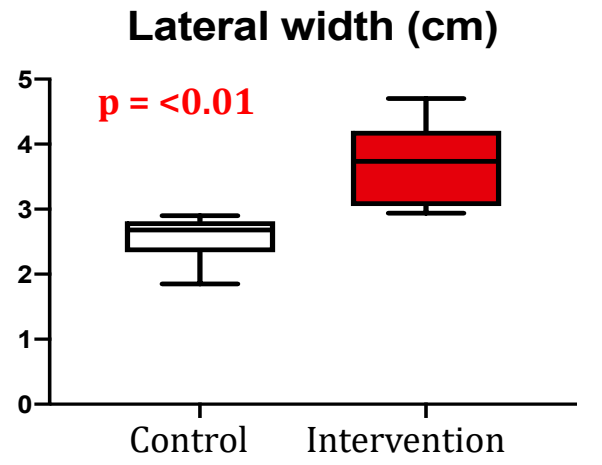

B)

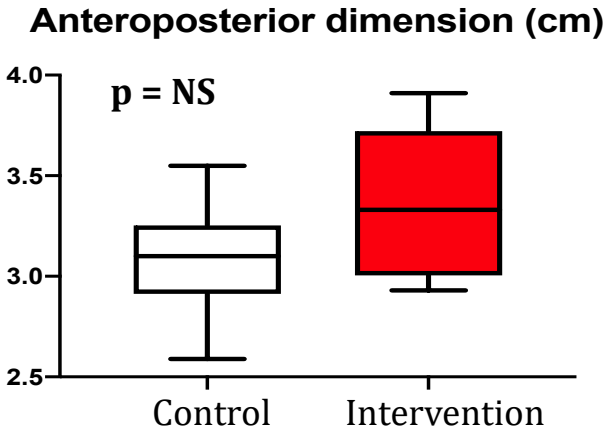

C)

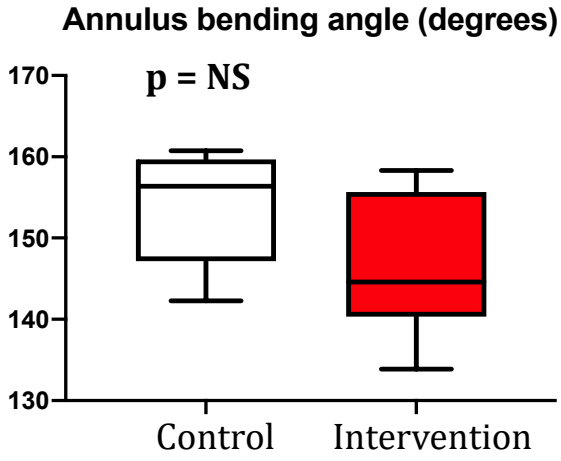

Figure 7: Key findings from 3DE regarding changes in TV annular geometry secondary to increased right ventricular volume and pressure loading. The TV annulus dilated more in the lateral width direction (A) than the anteroposterior direction (B). The annular bending angle was not significantly different (C).

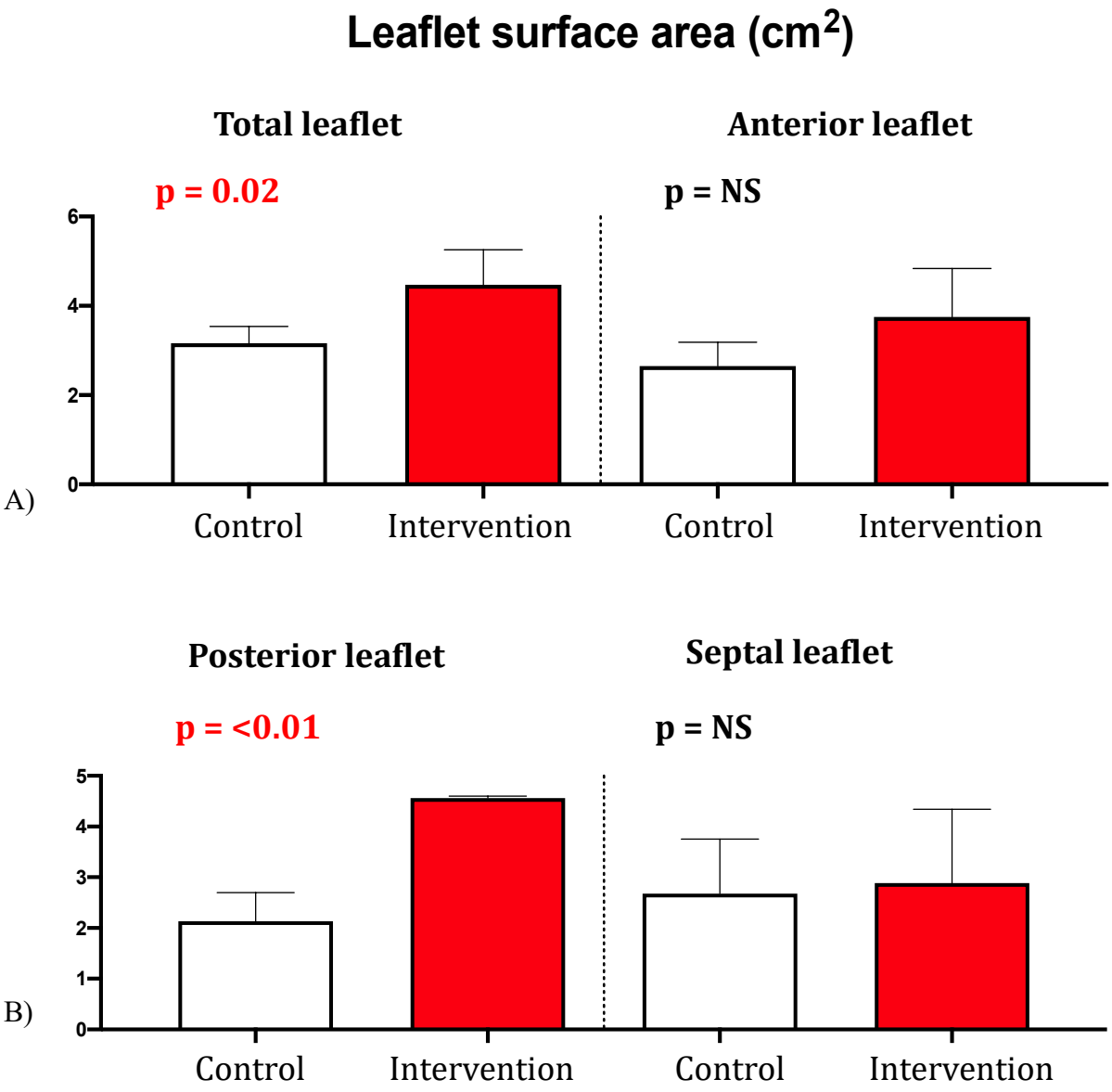

Figure 8: Changes in TV leaflet area as assessed on 3DE in response to increased right ventricular volume and pressure loading. There is increased total leaflet area (A) with proportionately more expansion of the posterior leaflet (B).

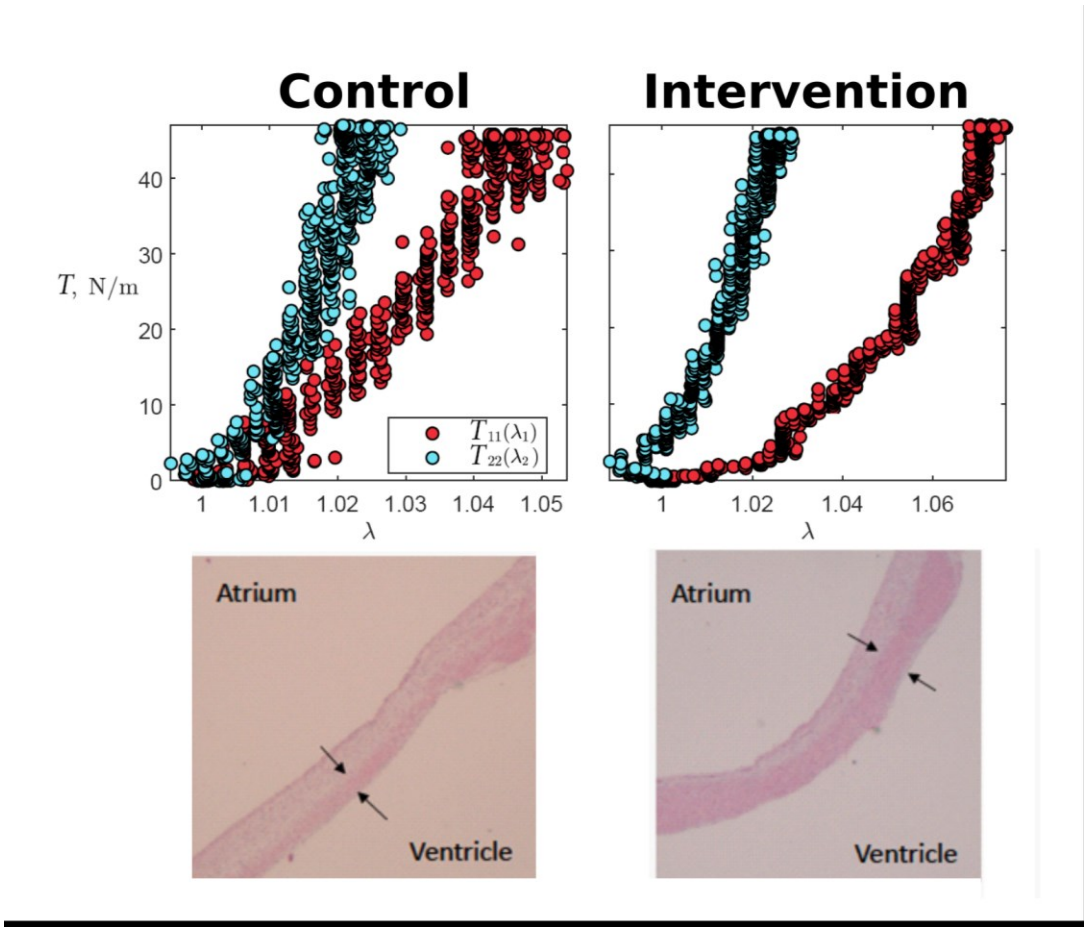

Figure 9: Representative membrane tension-stretch curves for CP and IP (top 2 panels). Direction 11 (red dots) is circumferential and 22 (green dots) is in the radial direction. Representative photograph of H&E sides with the fibrosa layer outlined in between the black arrows (bottom 2 panels).

Tables

Table 1. Comparisons of hemodynamic, echocardiographic pathologic parameters between intervention and control piglet groups for model validation. Values expressed as median (25^{th}, 75^{th} percentile) with Mann-Whitney U test p-values reported.

Parameters	Control Piglets	Intervention Piglets	P-value
Weight (kg)	33.8 (28.1, 36.3)	31.7 (27.7. 37.5)	NS
RV systolic pressure/arterial systolic pressure (%)	30.0 (28.8, 33.3)	78.0 (64.8, 82.5)	<0.001
Pulmonary regurgitation grade (0-4)	1.0 (1.0, 1.0)	4.0 (3.4, 4.0)	<0.001
Tricuspid regurgitation grade (0-4)	2.0 (1.4, 2.0)	3.0 (2.0, 3.6)	0.02
RV wall thickness (mm)	4.3 (4.0, 5.1)	9.3 (8.9, 11.0)	<0.001
Anterior papillary muscle cross-sectional area (cm2)	0.4 (0.3, 0.5)	1.1 (0.9, 1.5)	<0.001
RV Fractional Area Change (%)	49.3 (47.7, 55.9)	32.5 (26.1, 40.5)	<0.001

NS denotes non-significance.

Table 2. Comparisons of 3D echocardiographic (3DE) parameters and pathologic leaflet measurements between intervention and control piglet groups. Values expressed as median (25^{th}, 75^{th} percentile) with Mann-Whitney U test p-values reported.

3DE Parameters	Control Piglets	Intervention Piglets	P-value
In-vivo annular geometry			
TV annulus lateral width (cm)	2.7 (2.3, 2.8)	3.7 (3.0, 4.2)	<0.001
TV annulus anteroposterior dimension (cm)	3.1 (2.9, 3.3)	3.3 (3.0, 3.7)	NS
TV annulus width/anteroposterior dimension ratio	0.8 (0.7, 0.9)	1.0 (1.0, 1.2)	<0.001
TV annulus bending angle (degrees)	156 (147, 160)	145 (140, 156)	NS
In-vivo leaflet geometry			
TV Leaflet Area (cm2) at mid-systole	7.7 (5.8, 8.5)	11.0 (7.5, 13.7)	0.02
Anterior Leaflet Area (cm2)	2.6 (1.7, 3.2)	3.8 (2.3, 4.8)	NS
Posterior Leaflet Area (cm2)	2.1 (1.5, 2.7)	4.6 (2.6, 4.6)	0.004
Septal Leaflet Area (cm2)	2.7 (1.8, 3.8)	2.9 (2.5, 4.3)	NS
TV Prolapse volume (ml) at mid-systole	0.008 (0.0009, 0.03)	0.003 (0.0005, 0.007)	NS
TV Tethering volume (ml) at mid systole	1.1 (0.9, 1.7)	2.9 (1.8, 4.6)	0.02
TV Leaflet Area (cm2) at end-systole	7.8 (6.7, 9.6)	11.9 (7.9, 15.1)	0.02
TV Coaptation Index	0.07 (0.05, 0.2)	0.08 (0.02, 0.2)	NS
TV Tenting height (cm)	0.7 (0.5, 0.7)	0.8 (0.5, 1.0)	NS
In-vivo anterior papillary muscle geometry			
PM angle to 90º of annulus plane (degree)	17.7 (14.7, 30.0)	15.4 (5.5, 22.3)	NS
Chordal length (cm)	1.0 (0.9, 1.1)	1.2 (1.1, 1.3)	0.04
PM length (cm)	1.6 (1.4, 2.0)	2.3 (1.7, 2.7)	NS
Anterior papillary muscle cross-sectional area (cm2)	0.4 (0.3, 0.5)	1.1 (0.9, 1.5)	<0.001
Ex-vivo leaflet area			
TV leaflet area (cm2) measured in relaxed state	11.6 (10.2, 13.8)	12.3 (10.4, 14.5)	NS
Anterior Leaflet Area (cm2)	4.0 (3.6, 4.8)	4.1 (3.5, 4.9)	NS
Posterior Leaflet Area (cm2)	4.1 (3.6, 4.6)	4.6 (3.4, 5.3)	NS
Septal Leaflet Area (cm2)	3.0 (2.7, 3.3)	3.5 (2.9, 4.1)	NS

NS denotes non-significance.

References

[1] Bokma JP, Winter MM, Oosterhof T, Vliegen HW, Van Dijk AP, Hazekamp MG, et al. Severe tricuspid regurgitation is predictive for adverse events in tetralogy of Fallot. Heart 2015;101:794–799. doi:10.1136/heartjnl-2014-306919.

[2] Wertaschnigg D, Manlhiot C, Jaeggi M, Seed M, Dragulescu A, Schwartz SM, et al. Contemporary Outcomes and Factors Associated With Mortality After a Fetal or Neonatal Diagnosis of Ebstein Anomaly and Tricuspid Valve Disease. Can J Cardiol 2016;32:1500–1506. doi:10.1016/j.cjca.2016.03.008.

[3] De León LE, Mery CM, Verm RA, Trujillo-Díaz D, Patro A, Guzmán-Pruneda FA, et al. Mid-Term Outcomes in Patients with Congenitally Corrected Transposition of the Great Arteries: A Single Center Experience. J Am Coll Surg 2017;224:707–715. doi:10.1016/j.jamcollsurg.2016.12.029.

[4] Agnetti a, Carano N, Cavalli C, Tchana B, Bini M, Squarcia U, et al. Long-term outcome after senning operation for transposition of the great arteries. Clin Cardiol 2004;27:611–614.

[5] Chen L, Larsen CM, Le RJ, Connolly HM, Pislaru S V., Murphy JG, et al. The prognostic significance of tricuspid valve regurgitation in pulmonary arterial hypertension. Clin Respir J 2018;12:1572–1580. doi:10.1111/crj.12713.

[6] Alsaied T, Bokma JP, Engel ME, Kuijpers JM, Hanke SP, Zuhlke L, et al. Factors associated with long-term mortality after Fontan procedures: A systematic review. Heart 2017;103:104–110. doi:10.1136/heartjnl-2016-310108.

[7] Dean PN, Hillman DG, McHugh KE, Gutgesell HP. Inpatient Costs and Charges for Surgical Treatment of Hypoplastic Left Heart Syndrome. Pediatrics

2011;128:e1181–e1186. doi:10.1542/peds.2010-3742.

[8] Barber G, Helton JG, Aglira BA, Chin AJ, Murphy JD, Pigott JD, et al. The significance of tricuspid regurgitation in hypoplastic left-heart syndrome. Am Heart J 1988;116:1563–1567. doi:10.1016/0002-8703(88)90744-2.

[9] Elmi M, Hickey EJ, Williams WG, Van Arsdell G, Caldarone CA, McCrindle BW. Long-term tricuspid valve function after Norwood operation. J Thorac Cardiovasc Surg 2011;142:1341-1347.e4. doi:10.1016/j.jtcvs.2010.11.065.

[10] Bartram U, Grünenfelder J, Van Praagh R. Causes of death after the modified Norwood procedure: A study of 122 postmortem cases. Ann Thorac Surg 1997;64:1795–1802. doi:10.1016/S0003-4975(97)01041-2.

[11] Hehir DA, Dominguez TE, Ballweg JA, Ravishankar C, Marino BS, Bird GL, et al. Risk factors for interstage death after stage 1 reconstruction of hypoplastic left heart syndrome and variants. J Thorac Cardiovasc Surg 2008;136:19–25. doi:10.1016/j.jtcvs.2007.12.012.

[12] Honjo O, Atlin CR, Mertens L, Al-Radi OO, Redington AN, Caldarone CA, et al. Atrioventricular valve repair in patients with functional single-ventricle physiology: Impact of ventricular and valve function and morphology on survival and reintervention. J Thorac Cardiovasc Surg 2011;142:326-335.e2. doi:10.1016/j.jtcvs.2010.11.060.

[13] Pundi KN, Johnson JN, Dearani JA, Pundi KN, Li Z, Hinck CA, et al. 40-Year Follow-Up after the Fontan Operation Long-Term Outcomes of 1,052 Patients. J Am Coll Cardiol 2015;66:1700–1710. doi:10.1016/j.jacc.2015.07.065.

[14] Ono M, Cleuziou J, Pabst von Ohain J, Beran E, Burri M, Strbad M, et al.

Atrioventricular valve regurgitation in patients undergoing total cavopulmonary connection: Impact of valve morphology and underlying mechanisms on survival and reintervention. J Thorac Cardiovasc Surg 2018;155:701-709.e6. doi:10.1016/j.jtcvs.2017.08.122.

[15] King G, Ayer J, Celermajer D, Zentner D, Justo R, Disney P, et al. Atrioventricular Valve Failure in Fontan Palliation. J Am Coll Cardiol 2019;73:810–822. doi:10.1016/j.jacc.2018.12.025.

[16] Mosca RS, Bove EL. Tricuspid Valvuloplasty in Hypoplastic Left Heart Syndrome. Semin Thorac Cardiovasc Surg Pediatr Card Surg Annu 1999;2:21–34. doi:10.1016/s1092-9126(99)70003-7.

[17] Kanani M, Moorman AFM, Cook AC, Webb S, Brown NA, Lamers WH, et al. Development of the atrioventricular valves: Clinicomorphological correlations. Ann Thorac Surg 2005;79:1797–1804. doi:10.1016/j.athoracsur.2004.06.122.

[18] Lamers WH, Virágh S, Wessels A, Moorman AF, Anderson RH. Formation of the tricuspid valve in the human heart. Circulation 1995;91:111–121. doi:10.1161/01.CIR.91.1.111.

[19] de Vlaming A, Sauls K, Hajdu Z, Visconti RP, Mehesz AN, Levine RA, et al. Atrioventricular valve development: New perspectives on an old theme. Differentiation 2012;84:103–116. doi:10.1016/j.diff.2012.04.001.

[20] Eisenberg LM, Markwald RR. Molecular regulation of atrioventricular valvuloseptal morphogenesis. Circ Res 1995;77:1–6. doi:10.1161/01.RES.77.1.1.

[21] Person AD, Klewer SE, Runyan RB. Cell biology of cardiac cushion development. Int Rev Cytol 2005;243:287–335. doi:10.1016/S0074-7696(05)43005-3.

[22] Combs MD, Yutzey KE. Heart valve development: Regulatory networks in development and disease. Circ Res 2009;105:408–421. doi:10.1161/CIRCRESAHA.109.201566.

[23] Eisenberg LM, Markwald RR. Molecular regulation of atrioventricular valvuloseptal morphogenesis. Circ Res 1995;77:1–6. doi:10.1161/01.RES.77.1.1.

[24] Snarr BS, Kern CB, Wessels A. Origin and fate of cardiac mesenchyme. Dev Dyn 2008;237:2804–2819. doi:10.1002/dvdy.21725.

[25] Kim JS, Virágh S, Moorman AFM, Anderson RH, Lamers WH. Development of the myocardium of the atrioventricular canal and the vestibular spine in the human heart. Circ Res 2001;88:395–402. doi:10.1161/01.RES.88.4.395.

[26] Wessels A, Markman MWM, Vermeulen JLM, Anderson RH, Moorman AFM, Lamers WH. The development of the atrioventricular junction in the human heart. Circ Res 1996;78:110–117. doi:10.1161/01.RES.78.1.110.

[27] De Lange FJ, Moorman AFM, Anderson RH, Männer J, Soufan AT, De Gier-De Vries C, et al. Lineage and morphogenetic analysis of the cardiac valves. Circ Res 2004;95:645–654. doi:10.1161/01.RES.0000141429.13560.cb.

[28] Anderson RH, Webb S, Brown NA, Lamers W, Moorman A. Development of the heart: (2) Septation of the atriums and ventricles. Heart 2003;89:949–958.

[29] De Lange FJ, Moorman AFM, Anderson RH, Männer J, Soufan AT, De Gier-De Vries C, et al. Lineage and morphogenetic analysis of the cardiac valves. Circ Res 2004;95:645–654. doi:10.1161/01.RES.0000141429.13560.cb.

[30] Lin CJ, Lin CY, Chen CH, Zhou B, Chang CP. Partitioning the heart: Mechanisms of cardiac septation and valve development. Dev 2012;139:3277–3299.

doi:10.1242/dev.063495.

[31] Kruithof BPT, Krawitz SA, Gaussin V. Atrioventricular valve development during late embryonic and postnatal stages involves condensation and extracellular matrix remodeling. Dev Biol 2007;302:208–217. doi:10.1016/j.ydbio.2006.09.024.

[32] Levine RA, Hagége AA, Judge DP, Padala M, Dal-Bianco JP, Aikawa E, et al. Mitral valve disease-morphology and mechanisms. Nat Rev Cardiol 2015;12:689–710. doi:10.1038/nrcardio.2015.161.

[33] Lincoln J, Alfieri CM, Yutzey KE. Development of heart valve leaflets and supporting apparatus in chicken and mouse embryos. Dev Dyn 2004;230:239–250. doi:10.1002/dvdy.20051.

[34] Oosthoek PW, Wenink ACG, Wisse LJ, Gittenberger-de Groot AC. Development of the papillary muscles of the mitral valve: Morphogenetic background of parachute-like asymmetric mitral valves and other mitral valve anomalies. J Thorac Cardiovasc Surg 1998;116:36–46. doi:10.1016/S0022-5223(98)70240-5.

[35] Rogers JH, Bolling SF. The tricuspid valve: Current perspective and evolving management of tricuspid regurgitation. Circulation 2009;119:2718–2725. doi:10.1161/CIRCULATIONAHA.108.842773.

[36] Nii M, Roman KS, Macgowan CK, Smallhorn JF. Insight into normal mitral and tricuspid annular dynamics in pediatrics: A real-time three-dimensional echocardiographic study. J Am Soc Echocardiogr 2005;18:805–814. doi:10.1016/j.echo.2005.01.014.

[37] Nii M, Guerra V, Roman KS, Macgowan CK, Smallhorn JF. Three-dimensional Tricuspid Annular Function Provides Insight into the Mechanisms of Tricuspid

Valve Regurgitation in Classic Hypoplastic Left Heart Syndrome. J Am Soc Echocardiogr 2006;19:391–402. doi:10.1016/j.echo.2005.10.025.

[38] Silver MD, Lam JH, Ranganathan N, Wigle ED. Morphology of the human tricuspid valve. Circulation 1971;43:333–348. doi:10.1161/01.CIR.43.3.333.

[39] Wafae N, Hayashi H, Gerola L, Vieira M. Anatomical study of the human tricuspid valve. Surg Radiol Anat 1990;12:37–41.

[40] Tretter JT, Friedberg MK, Wald RM, McElhinney DB. Defining and refining indications for transcatheter pulmonary valve replacement in patients with repaired tetralogy of Fallot: Contributions from anatomical and functional imaging. Int J Cardiol 2016;221:916–925. doi:10.1016/j.ijcard.2016.07.120.

[41] Restivo A, Smith A, Wilkinson JL, Anderson RH. The medial papillary muscle complex and its related septomarginal trabeculation. A normal anatomical study on human hearts. J Anat 1989;163:231–242.

[42] Nigri GR, Di Dio LJA, Baptista CAC. Papillary muscles and tendinous cords of the right ventricle of the human heart: Morphological characteristics. Surg Radiol Anat 2001;23:45–49. doi:10.1007/s00276-001-0045-7.

[43] Loukas M, Shane Tubbs R, Louis RG, Apaydin N, Bartczak A, Huseng V, et al. An endoscopic and anatomical approach to the septal papillary muscle of the conus. Surg Radiol Anat 2009;31:701–706. doi:10.1007/s00276-009-0510-2.

[44] Tretter JT, Sarwark AE, Anderson RH, Spicer DE. Assessment of the anatomical variation to be found in the normal tricuspid valve. Clin Anat 2016;29:399–407. doi:10.1002/ca.22591.

[45] Saha A, Roy S. Papillary muscles of right ventricle—morphological variations and

its clinical relevance. Cardiovasc Pathol 2018;34:22–27. doi:10.1016/j.carpath.2018.01.007.

[46] Muresian H. The clinical anatomy of the right ventricle. Clin Anat 2016;29:380–398. doi:10.1002/ca.22484.

[47] Martinez RM, O'Leary PW, Anderson RH. Anatomy and echocardiography of the normal and abnormal tricuspid valve. Cardiol Young 2006;16:4–11. doi:10.1017/S1047951106000709.

[48] Muresian H. The clinical anatomy of the right ventricle. Clin Anat 2016;29:380–398. doi:10.1002/ca.22484.

[49] Wenink ACG. The medial papillary complex. Heart 1977;39:1012–1018. doi:10.1136/hrt.39.9.1012.

[50] Aktas EO, Govsa F, Kocak A, Boydak B, Yavuz IC. Variations in the papillary muscles of normal tricuspid valve and their clinical relevance in medicolegal autopsies. Saudi Med J 2004;25:1176–1185.

[51] Thiene G, Daliento L, Frescura C, De Tommasi M, Macartney FJ, Anderson RH. Atresia of left atrioventricular orifice. Anatomical investigation in 62 cases. Br Heart J 1981;45:393–401.

[52] Stamm C, Anderson RH, Ho SY. The morphologically tricuspid valve in hypoplastic left heart syndrome. Eur J Cardio-Thoracic Surg 1997;12:587–592. doi:10.1016/S1010-7940(97)00184-X.

[53] Kutty S, Colen T, Thompson RB, Tham E, Li L, Vijarnsorn C, et al. Tricuspid regurgitation in hypoplastic left heart syndrome mechanistic insights from 3-dimensional echocardiography and relationship with outcomes. Circ Cardiovasc

Imaging 2014;7:765–772. doi:10.1161/CIRCIMAGING.113.001161.

[54] Takahashi K, Inage A, Rebeyka IM, Ross DB, Thompson RB, MacKie AS, et al. Real-time 3-dimensional echocardiography provides new insight into mechanisms of tricuspid valve regurgitation in patients with hypoplastic left heart syndrome. Circulation 2009;120:1091–1098. doi:10.1161/CIRCULATIONAHA.108.809566.

[55] Khoo NS, Smallhorn JF, Kaneko S, Myers K, Kutty S, Tham EB. Novel insights into RV adaptation and function in hypoplastic left heart syndrome between the first 2 stages of surgical palliation. JACC Cardiovasc Imaging 2011;4:128–137. doi:10.1016/j.jcmg.2010.09.022.

[56] Januszewska K, Kozlik-Feldmann R, Kordon Z, Urschel S, Netz H, Reichart B, et al. Significance of the residual aortic obstruction in multistage repair of hypoplastic left heart syndrome. Eur J Cardio-Thoracic Surg 2011;40:508–513. doi:10.1016/j.ejcts.2010.12.023.

[57] Bharucha T, Honjo O, Seller N, Atlin C, Redington A, Caldarone CA, et al. Mechanisms of tricuspid valve regurgitation in hypoplastic left heart syndrome: A case-matched echocardiographic-surgical comparison study. Eur Heart J Cardiovasc Imaging 2013;14:135–141. doi:10.1093/ehjci/jes123.

[58] Bharucha T, Khan R, Mertens L, Friedberg MK. Right ventricular mechanical dyssynchrony and asymmetric contraction in hypoplastic heart syndrome are associated with tricuspid regurgitation. J Am Soc Echocardiogr 2013;26:1214–1220. doi:10.1016/j.echo.2013.06.015.

[59] Reed GE, Cortes LE. Measured Tricuspid Annuloplasty: A Rapid and Reproducible Technique. Ann Thorac Surg 1976;21:168–169. doi:10.1016/S0003-

4975(10)64283-X.

[60] Kay JH, Mendez AM, Zubiate P. A Further Look at Tricuspid Annuloplasty. Ann Thorac Surg 1976;22:498–500. doi:10.1016/S0003-4975(10)64462-1.

[61] Ohye RG, Gomez CA, Goldberg CS, Graves HL, Devaney EJ, Bove EL. Tricuspid valve repair in hypoplastic left heart syndrome. J Thorac Cardiovasc Surg 2004;127:465–472.

[62] Bove EL, Ohye RG, Devaney EJ, Hirsch J. Tricuspid Valve Repair for Hypoplastic Left Heart Syndrome and the Failing Right Ventricle. Pediatr Card Surg Annu 2007;10:101–104. doi:10.1053/j.pcsu.2007.01.020.

[63] Dinh DC, Gurney JG, Donohue JE, Bove EL, Hirsch JC, Devaney EJ, et al. Tricuspid valve repair in hypoplastic left heart syndrome. Pediatr Cardiol 2011;32:599–606. doi:10.1007/s00246-011-9924-9.

[64] Tsang VT, Raja SG. Tricuspid Valve Repair in Single Ventricle: Timing and Techniques. Semin Thorac Cardiovasc Surg Pediatr Card Surg Annu 2012;15:61–68. doi:10.1053/j.pcsu.2012.01.010.

[65] Alsoufi B, Sinha R, McCracken C, Figueroa J, Altin F, Kanter K. Outcomes and risk factors associated with tricuspid valve repair in children with hypoplastic left heart syndrome†. Eur J Cardio-Thoracic Surg 2018;54:993–1000. doi:10.1093/ejcts/ezy198.

[66] Sasaki T, Takahashi Y, Ando M, Wada N. Edge-to-edge tricuspid valve repair in hypoplastic left heart syndrome. Gen Thorac Cardiovasc Surg 2007;155:505–507. doi:10.1007/s11748-007-0176-9.

[67] Ando M, Takahashi Y. Edge-to-Edge Repair of Common Atrioventricular or

Tricuspid Valve in Patients With Functionally Single Ventricle. Ann Thorac Surg 2007;84:1571–1577. doi:10.1016/j.athoracsur.2007.06.026.

[68] Bautista-Hernandez V, Brown DW, Loyola H, Myers PO, Borisuk M, Del Nido PJ, et al. Mechanisms of tricuspid regurgitation in patients with hypoplastic left heart syndrome undergoing tricuspid valvuloplasty. J Thorac Cardiovasc Surg 2014;148:832–840. doi:10.1016/j.jtcvs.2014.06.044.

[69] Ruzmetov M, Welke KF, Geiss DM, Fortuna RS. Outcomes of tricuspid valve repair in children with hypoplastic left heart syndrome. J Card Surg 2014;29:698–704. doi:10.1111/jocs.12414.

[70] Sugiura J, Nakano T, Oda S, Usui A, Ueda Y, Kado H. Effects of tricuspid valve surgery on tricuspid regurgitation in patients with hypoplastic left heart syndrome: A non-randomized series comparing surgical and non-surgical cases. Eur J Cardio-Thoracic Surg 2014;46:8–13. doi:10.1093/ejcts/ezt613.

[71] Ugaki S, Khoo NS, Ross DB, Rebeyka IM, Adatia I. Tricuspid valve repair improves early right ventricular and tricuspid valve remodeling in patients with hypoplastic left heart syndrome. J Thorac Cardiovasc Surg 2013;145:446–450. doi:10.1016/j.jtcvs.2012.10.040.

[72] Ugaki S, Khoo NS, Ross DB, Rebeyka IM, Adatia I. Right ventricular and tricuspid valve remodeling after bidirectional cavopulmonary anastomosis. Circ J 2013;77:2514–2518. doi:10.1253/circj.CJ-12-1635.

[73] Dal-Bianco JP, Aikawa E, Bischoff J, Guerrero JL, Handschumacher MD, Sullivan S, et al. Active adaptation of the tethered mitral valve: Insights into a compensatory mechanism for functional mitral regurgitation. Circulation

2009;120:334–342. doi:10.1161/CIRCULATIONAHA.108.846782.

[74] Sonnenblick EH, Napolitano LM, Daggett WM, Cooper T. An intrinsic neuromuscular basis for mitral valve motion in the dog. Circ Res 1967;21:9–15. doi:10.1161/01.RES.21.1.9.

[75] Krishnamurthy G, Itoh A, Swanson JC, Bothe W, Karlsson M, Kuhl E, et al. Regional stiffening of the mitral valve anterior leaflet in the beating ovine heart. J Biomech 2009;42:2697–2701. doi:10.1016/j.jbiomech.2009.08.028.

[76] Swanson JC, Krishnamurthy G, Itoh A, Escobar Kvitting JP, Bothe W, Craig Miller D, et al. Multiple mitral leaflet contractile systems in the beating heart. J Biomech 2011;44:1328–1333. doi:10.1016/j.jbiomech.2011.01.006.

[77] Marron K, Yacoub MH, Polak JM, Sheppard MN, Fagan D, Whitehead BF, et al. Innervation of human atrioventricular and arterial valves. Circulation 1996;94:368–375. doi:10.1161/01.CIR.94.3.368.

[78] De Biasi S, Vitellaro-Zuccarello L, Blum I. Histochemical and ultrastructural study on the innervation of human and porcine atrio-ventricular valves. Anat Embryol (Berl) 1984;169:159–165.

[79] Krishnamurthy G, Ennis DB, Itoh A, Bothe W, Swanson JC, Karlsson M, et al. Material properties of the ovine mitral valve anterior leaflet in vivo from inverse finite element analysis. AJP Hear Circ Physiol 2008;295:H1141–H1149. doi:10.1152/ajpheart.00284.2008.

[80] Itoh A, Krishnamurthy G, Swanson JC, Ennis DB, Bothe W, Kuhl E, et al. Active stiffening of mitral valve leaflets in the beating heart. AJP Hear Circ Physiol 2009;296:H1766–H1773. doi:10.1152/ajpheart.00120.2009.

[81] Swanson JC, Krishnamurthy G, Kvitting J-PE, Craig Miller D, Ingels NB. Electromechanical coupling between the atria and mitral valve. Am J Physiol Circ Physiol 2011;300:H1267–H1273. doi:10.1152/ajpheart.00971.2010.

[82] Pucéat M. Embryological origin of the endocardium and derived valve progenitor cells: From developmental biology to stem cell-based valve repair. Biochim Biophys Acta - Mol Cell Res 2013;1833:917–922. doi:10.1016/j.bbamcr.2012.09.013.

[83] Colen T, Kutty S, Thompson RB, Tham E, Mackie AS, Li L, et al. Tricuspid Valve Adaptation during the First Interstage Period in Hypoplastic Left Heart Syndrome. J Am Soc Echocardiogr 2018;31:624–633. doi:10.1016/j.echo.2017.11.020.

[84] Ricci M, Lombardi P, Galindo A, Schultz S, Vasquez A, Rosenkranz E. Effects of single-ventricle physiology with aortopulmonary shunt on regional myocardial blood flow in a piglet model. J Thorac Cardiovasc Surg 2006;132. doi:10.1016/j.jtcvs.2006.03.050.

[85] Merklinger SL, Honjo O, Al-Radi OO, Poe J, Wang J, Oka N, et al. Primary in-series palliation of hypoplastic left heart syndrome with mechanical lung assist in neonatal pigs. ASAIO J 2009;55:620–625. doi:10.1097/MAT.0b013e3181be00a0.

[86] Holzer RJ, Green J, Bergdall V, Chisolm JL, Hill SL, Galantowicz M, et al. An animal model for hybrid stage i palliation of hypoplastic left heart syndrome. Pediatr Cardiol 2009;30:922–927. doi:10.1007/s00246-009-9463-9.

[87] Duginski GA, Ross CJ, Laurence DW, Johns CH, Lee C-H. An investigation of the effect of freezing storage on the biaxial mechanical properties of excised porcine tricuspid valve anterior leaflets. J Mech Behav Biomed Mater 2020;101:103438.

doi:10.1016/j.jmbbm.2019.103438.

[88] Ramsden CA, Reynolds EOR. Ventilator settings for newborn infants. Arch Dis Child 1987;62:976. doi:10.1136/adc.62.9.976-a.

[89] Salgo IS, Gorman JH, Gorman RC, Jackson BM, Bowen FW, Plappert T, et al. Effect of annular shape on leaflet curvature in reducing mitral leaflet stress. Circulation 2002;106:711–717. doi:10.1161/01.CIR.0000025426.39426.83.

[90] Kutty S, Colen T, Thompson RB, Tham E, Li L, Vijarnsorn C, et al. Tricuspid regurgitation in hypoplastic left heart syndrome mechanistic insights from 3-dimensional echocardiography and relationship with outcomes. Circ Cardiovasc Imaging 2014;7:765–772. doi:10.1161/CIRCIMAGING.113.001161.

[91] Hinton RB, Yutzey KE. Heart Valve Structure and Function in Development and Disease. Annu Rev Physiol 2011;73:29–46. doi:10.1146/annurev-physiol-012110-142145.

[92] Sacks MS, Merrryman WD, Schmidt DE. On the Biomechanics of Heart Valve. J Biomech 2010;42:1804–1824. doi:10.1016/j.jbiomech.2009.05.015.ON.

[93] Simionescu DT, Chen J, Jaeggli M, Wang B, Liao J. Form follows function: Advances in trilayered structure replication for aortic heart valve tissue engineering. J Healthc Eng 2012;3:179–202. doi:10.1260/2040-2295.3.2.179.

[94] Amini Khoiy K, Biswas D, Decker TN, Asgarian KT, Loth F, Amini R. Surface Strains of Porcine Tricuspid Valve Septal Leaflets Measured in Ex Vivo Beating Hearts. J Biomech Eng 2016;138:111006. doi:10.1115/1.4034621.

[95] Jett S, Laurence D, Kunkel R, Babu AR, Kramer K, Baumwart R, et al. An investigation of the anisotropic mechanical properties and anatomical structure of

porcine atrioventricular heart valves. J Mech Behav Biomed Mater 2018;87:155–171. doi:10.1016/j.jmbbm.2018.07.024.

[96] Lanir Y. A structural theory for the homogeneous biaxial stress-strain relationships in flat collagenous tissues. J Biomech 1979;12:423–436. doi:10.1016/0021-9290(79)90027-7.

[97] Lanir Y. Constitutive equations for fibrous connective tissues. J Biomech 1983;16:1–12. doi:10.1016/0021-9290(83)90041-6.

[98] Laohachai K, Winlaw D, Sholler G, Veerappan S, Cole A, Ayer J. The Degree of Left Ventricular Hypoplasia Is Associated with Tricuspid Regurgitation Severity in Infants with Hypoplastic Left Heart Syndrome. Pediatr Cardiol 2019;40:1035–1040. doi:10.1007/s00246-019-02111-5.

[99] Laurence D, Ross C, Jett S, Johns C, Echols A, Baumwart R, et al. An investigation of regional variations in the biaxial mechanical properties and stress relaxation behaviors of porcine atrioventricular heart valve leaflets. J Biomech 2019;83:16–27. doi:10.1016/j.jbiomech.2018.11.015.

[100] Alavi SH, Sinha A, Steward E, Milliken JC, Kheradvar A. Load Dependent Extracellular Matrix Organization in Atrioventricular Heart Valves: Differences and Similarities. Am J Physiol Heart Circ Physiol 2015:ajpheart.00164.2015. doi:10.1152/ajpheart.00164.2015.

[101] Von Gise A, Pu WT. Endocardial and epicardial epithelial to mesenchymal transitions in heart development and disease. Circ Res 2012;110:1628–1645. doi:10.1161/CIRCRESAHA.111.259960.